Nano Today (2013) 8, 531—554

Available online at www.sciencedirect.com

ScienceDirect

journal homepage: www.elsevier.com/locate/nanotoday

REVIEW

Small power: Autonomous nano- and micromotors propelled by self-generated gradients

Wei Wang, Wentao Duan, Suzanne Ahmed, Thomas E. Mallouk*, Ayusman Sen*

Department of Chemistry, The Pennsylvania State University, University Park, PA 16802, United States

Received 4 July 2013 ; received in revised form 8 August 2013; accepted 30 August 2013
Available online 25 September 2013

KEYWORDS
Autonomous motor;
Self-electrophoresis;
Self-diffusiophoresis;
Self-acoustophoresis;
Self-generated fields;
Nanomotor

Summary In this article we review the development, current status and future prospects of nano- and microscale motors propelled by locally generated fields and chemical gradients. These motors move autonomously in fluids by converting different sources of energy into mechanical work. Most commonly they are particles that are similar in their largest dimensions to bacteria (a few microns) or eukaryotic cells (10—20 μm). Their shapes and compositions are designed to break symmetry in some way to create a local gradient (chemical, acoustic, thermal, *etc.*). A few important principles are introduced for readers to understand the physics of powered movement on small length scales. Interesting collective and emergent behaviors, as well as current and developing applications of these motors are also reviewed. Nano- and micromotors that are propelled by other mechanisms such as bubble recoil and magnetic induction are also briefly discussed.

Introduction

Motors and machines are so much a part of everyday life that it is hard to imagine a world without them. It is safe to say that machines powered by water, wind, electricity, and fuel have played a major role in the development of civilization, enabling human life at a scale that would not be possible without them. Motors are now deeply ingrained in almost every aspect of technology. Similarly, microscopic biological motors and machines are vital components of every living cell and organism. Chemically powered nanomotors in the cell are engaged in protein synthesis, DNA replication, ATP synthesis, cell division and motility. At the level of organisms, catalytic nanomotors power animal locomotion from the bumblebee to the blue whale. A representative illustration of synthetic and biological motors on different length scales is shown in Fig. 1.

Despite the ubiquity of engineered motors and machines in human life, and of nanomotors in biology, it is only recently that the concepts have begun to meet in the design of synthetic nano- and micromotors. Making

* Corresponding authors.
E-mail addresses: tom@chem.psu.edu (T.E. Mallouk), asen@psu.edu (A. Sen).

1748-0132/$ — see front matter © 2013 Elsevier Ltd. All rights reserved.
http://dx.doi.org/10.1016/j.nantod.2013.08.009

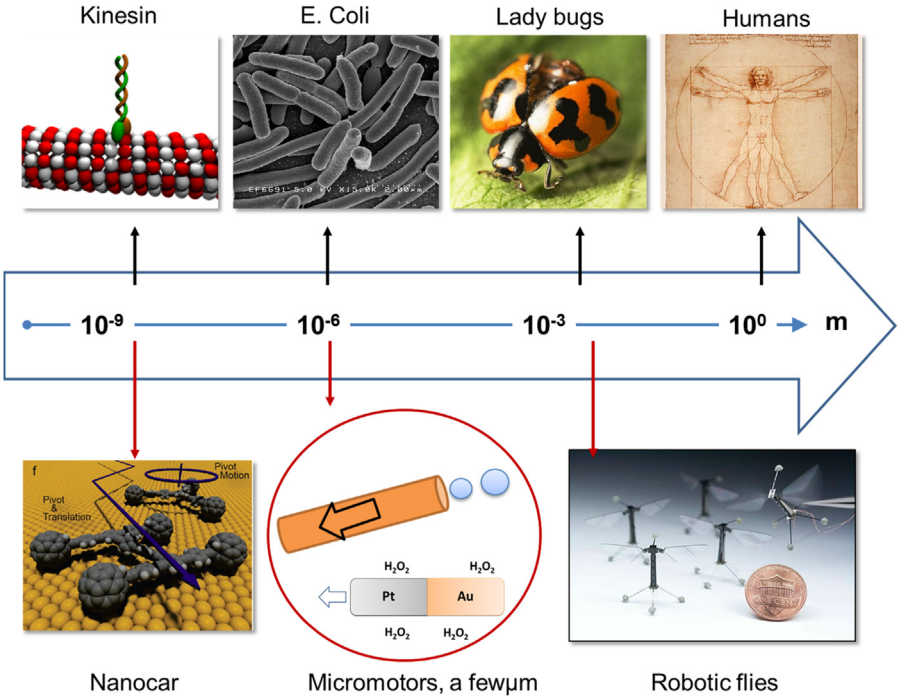

Figure 1 Natural (top) and synthetic (bottom) motors at different scales. The natural motors listed on the top row are: a kinesin on a microtubule (~10 nm) [1], a swarm of *E. coli* (a few μm) [2], a lady bug (a few mm) [3] and the Vitruvian man by Da Vinci (~2 m) [4]. The synthetic motors illustrated on the bottom row are: nanocars with C60 as wheels fabricated by the Tour group (a few nm) [5] (copyright 2005 The American Chemical Society), bubble propelled [6] and self-electrophoretic micromotors [7] (circled red, a few μm to tens of μm) and robotic insects fabricated by the Wood group (~1 cm) [8], copyright 2013 Science.

functional motors on the nano- and micrometer length scales is challenging, not only because it is difficult to fabricate structurally complex objects of this size, but because familiar macroscopic principles of powering them (*e.g.*, by electromagnetic induction, or by combustion of fuel to do pressure-volume work) do not scale down well. For example, the nanocar shown in Fig. 1 has fullerene wheels that actually roll on a gold surface, but no internal combustion engine to make them go.

Synthetic motors that are powered by self-generated gradients have been the subject of growing interest and study since their discovery in 2004 [7]. These motors can move autonomously in fluids at speeds up to millimeters per second, and in some cases can generate sufficient force to penetrate cell membranes. This article reviews recent progress and future prospects in this field.

Important concepts

In this section we present several concepts that are essential to the discussion of autonomous nano- and micromotors.

Reynolds number and Brownian motion

Not unlike their macroscale counterparts, motors functioning at nano- and microscale convert energy of various sources into mechanical motion. However the specific mechanisms for such energy conversion are usually dramatically different. At the macroscale objects can maintain their motion with inertia. However as the particle size decreases, inertia, which scales with L^3, becomes negligible compared to viscous forces that scale with L, where L is the characteristic length of the object. The Reynolds number (*Re*) is a dimensionless number that represents the ratio of these two forces:

$$Re = \frac{\rho v L}{\mu} \quad (1)$$

where ρ is density, v is the particle velocity and μ is the dynamic viscosity of the medium. A swimming person therefore has a Reynolds number of roughly 10^4 whereas bacteria have a Reynolds number of roughly 10^{-4}. For most of the nano- and microscale motors that will be discussed in this review, the Reynolds number will be on the same order as that of moving bacteria.

A low Reynolds number poses two immediate challenges for tiny swimmers. The first is that since inertia no longer effectively contributes to motion, there can only be instantaneous motion caused by instantaneous force. In other words, to maintain motion at low Reynolds number a constant force, be it chemical, electrical, magnetic or acoustic in nature, must be applied. Certain kinds of propulsion — such as recoil from chemically generated bubbles — are inefficient because the motor is subject to a recoil force only at the instant of bubble release. Motors based on the inertia of flywheels or other massive bodies would similarly be inefficient at the microscale. The second challenge is to design motors whose movement is *non-reciprocal*. A motor that has a simple back and forth motion, such as the hinged movement of a clamshell, will not generate net directional

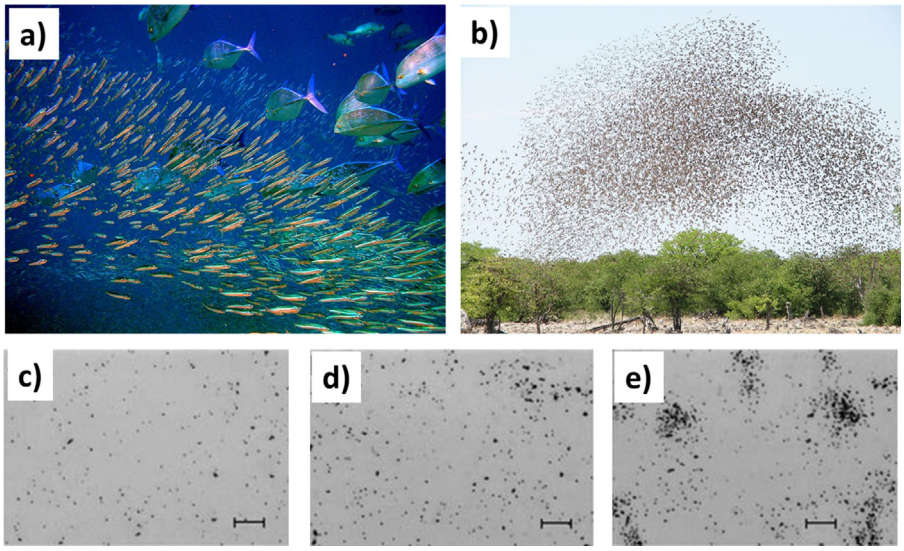

Figure 2 Related emergent behavior of biological organisms (a, b) and synthetic autonomous motors (c—e). (a) Schooling of anchovies [23]; (b) flocking of red billed queleas [24]; (c—e) schooling of AgCl microparticles under UV light (scale bar: 20 μm) [25]. Copyright 2009 John Wiley & Sons, Inc., reprinted with permission.

motion. This is called the ''scallop theorem'' [10]. In fact very rarely do nano-/micromotor designs involve moving parts [11—13]. In order to induce motion at low Reynolds number, symmetry needs to be broken, be it time-reversal symmetry, or symmetry in the particle composition, shape or surface reactions. Self-generated gradients, as will be the focus of this review, are commonly used by nano- and microscale motors, rotors and pumps as a means of breaking symmetry and inducing motion. Moreover surface (scaling with L^2) forces rather than body forces (scaling with L^3) dominate in inducing motion at small scales.

For motors at the nano- and microscale that function in aqueous media, collisions with water molecules become increasingly significant as their sizes decrease. Brownian motion induced by such collisions significantly interferes with the directionality of motors below 1 μm in size, and motors appear to diffuse randomly. In addition, the mechanism responsible for propulsion may become ineffective as the motor size decreases. Nature has developed various ways to achieve directional propulsion at the nano- and molecular levels, typically by embedding motors in membranes or by constraining them to travel on polymer chains to inhibit Brownian motion [14,15].

Autonomous *vs*. non-autonomous motors

Nano- and micromotors moving autonomously can be characterized by a trajectory that is independent of other motors. Each motor moves as if it has its own idea of a destination. This usually requires that the motors locally convert fuel or some excitation energy (light, sound, *etc.*), rather than be swept in a given direction by an externally applied field. Chemically propelled nano- and micromotors are typically autonomous. Their autonomy arises from the fact that each motor is itself a tiny engine that can convert chemical to mechanical energy.

External fields have been used to propel motors at nano- and microscale, most notably electric [16—18] and magnetic fields [19—22]. In most cases the external field is applied from a macroscopic source and exerts the same forces simultaneously on all the motors in the sample. Because the trajectories of motors propelled by magnetic and electric fields are usually dictated field lines, the resulting motion is generally not autonomous. A notable exception are the magnetic motors described by Dreyfus et al., who used a magnetic random force to generate a whiplike motion of a flagellar tail [10]. In 2012 we demonstrated that externally applied ultrasonic energy can induce autonomous motion of metal micro-rods [25]. In this system the scattering of acoustic energy generates a local pressure difference along the axis of the rod, which leads to autonomous motion.

Being able to move autonomously grants versatility to nano- and micromotors. Although external control is a much desired functionality for navigation and triggered response, autonomous motion is the foundation of collective behaviors such as swarming and schooling, an indication of inter-motor communication (Fig. 2). In addition it is beneficial to have motors that can independently carry out operations such as sensing and reporting, especially when different populations of motors have different tasks.

Motors, rotors and pumps

Autonomous nano- and micromachines can be divided into three major categories: motors that exhibit directional translational motion, rotors that follow circular trajectories, and pumps that stand still but drive the movement of fluids and tracer particles (Fig. 3).

These three types of micromachines break symmetry in different ways to induce movement. Micropumps break the symmetry of local concentrations of chemical species and fluid flow. Early micropump designs were based on self-electrophoresis/self-electroosmosis/ self-diffusiophoresis

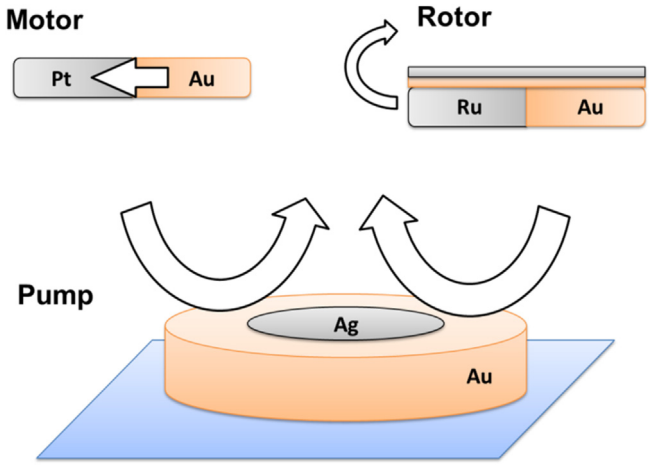

Figure 3 Catalytic micromotors, rotors and pumps. Electrocatalytic reactions of fuels in bi- and trimetallic structures of different designs can result in different kinds of micromachines such as motors [7], rotors [26] and pumps [27].

mechanisms [27—32]. Recent designs also include polymeric micropumps that function regardless of substrate materials, and pumps that take advantage of depolymerization reactions triggered by chemicals [33] or light [34]. Motors and rotors require a gradient (typically of proton concentration) along their body to generate motion. They are mostly rods or spheres with asymmetry in composition (*e.g.*, one side composed of active material and the other inert material) [35], activity (chemical reaction rate is higher at one side than the other) [7] or shape (two ends respond to the external field differently) [36]. The asymmetry is broken along one axis, which dictates the direction of motion. Nano- and microscale motors can become rotors if asymmetry (composition, shape or activity) is introduced perpendicular to the long axis of the particle instead of along the axis. There are a few examples of chemically propelled nano- and microrotors, and they are mostly rod-shaped [37—40]. Interestingly physical boundaries can also induce rotation [37]. External magnetic and electric fields, as well as light, can also be used to induce rotation of nano- and microparticles, however as in the case of motors, this rotation is generally not autonomous [41—43].

Propulsion mechanisms at nano- and microscale

Self-electrophoresis

Electrophoresis describes the transport of nano- and microscale particles in a liquid medium. In electrophoresis, charged particles migrate in and electric field (**E**), and their velocity (**U**) is governed by the Smoluchowsky equation for particles with thin double layers [44,45].

$$\mathbf{U} = \frac{\zeta_{rod}\varepsilon}{\mu}\mathbf{E} \quad (2)$$

here ζ_{rod} is the zeta potential of the rod surface which is related to the surface charge, ε is the permittivity of the medium (water), and μ is the dynamic viscosity of water.

Over the past ten years, many nano- and microscale motors have been designed to exploit the concept of electrophoresis. Unlike ordinary electrophoresis, these autonomous motors (particles) do not respond to an externally applied electric field; rather they generate a local electric field through chemical gradients and move in response to this self-generated electric field.

The first such system was discovered at Penn State [7], although at the time the mechanism of propulsion was not understood. In this system gold (Au)-platinum (Pt) nanorods (2—3 μm long and ~300 nm in diameter) were observed to move autonomously in dilute H_2O_2 (a few wt%) with Pt end leading at a speed of ~10 μm/s (Fig. 4a). The Ozin group independently made similar observations with gold-nickel nanorods of similar dimension [39] (Fig. 4b).

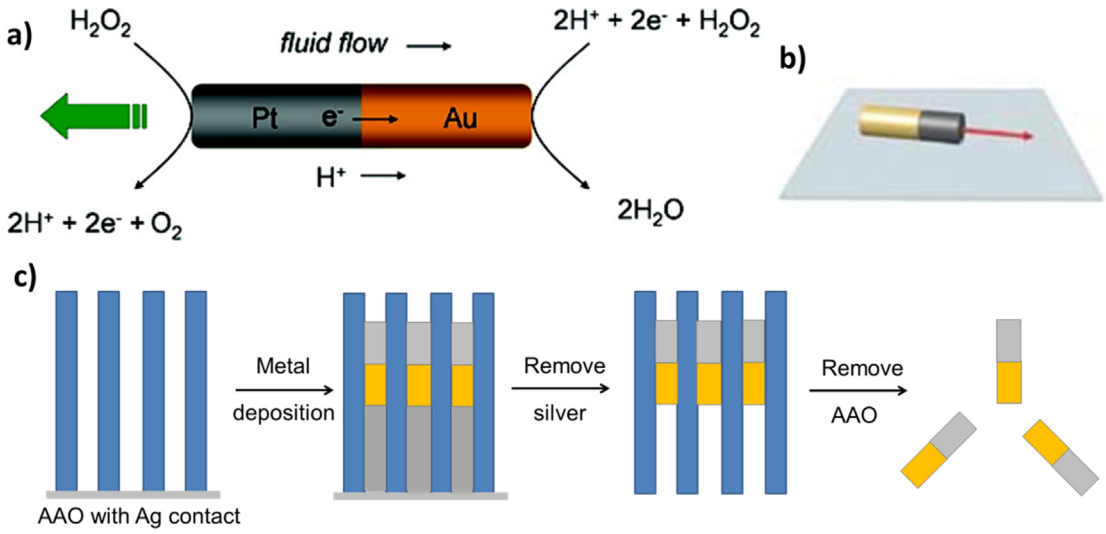

Figure 4 Early examples of rod shaped bimetallic nanomotors operating in H_2O_2 solutions. (a) Au—Pt nanorods [7], copyright 2004 The American Chemical Society, reprinted with permission; (b) Au—Ni nanorods [37], copyright 2010 John Wiley & Sons, Inc., reprinted with permission; (c) the template based electrodeposition process by which these bimetallic nanorods are made.

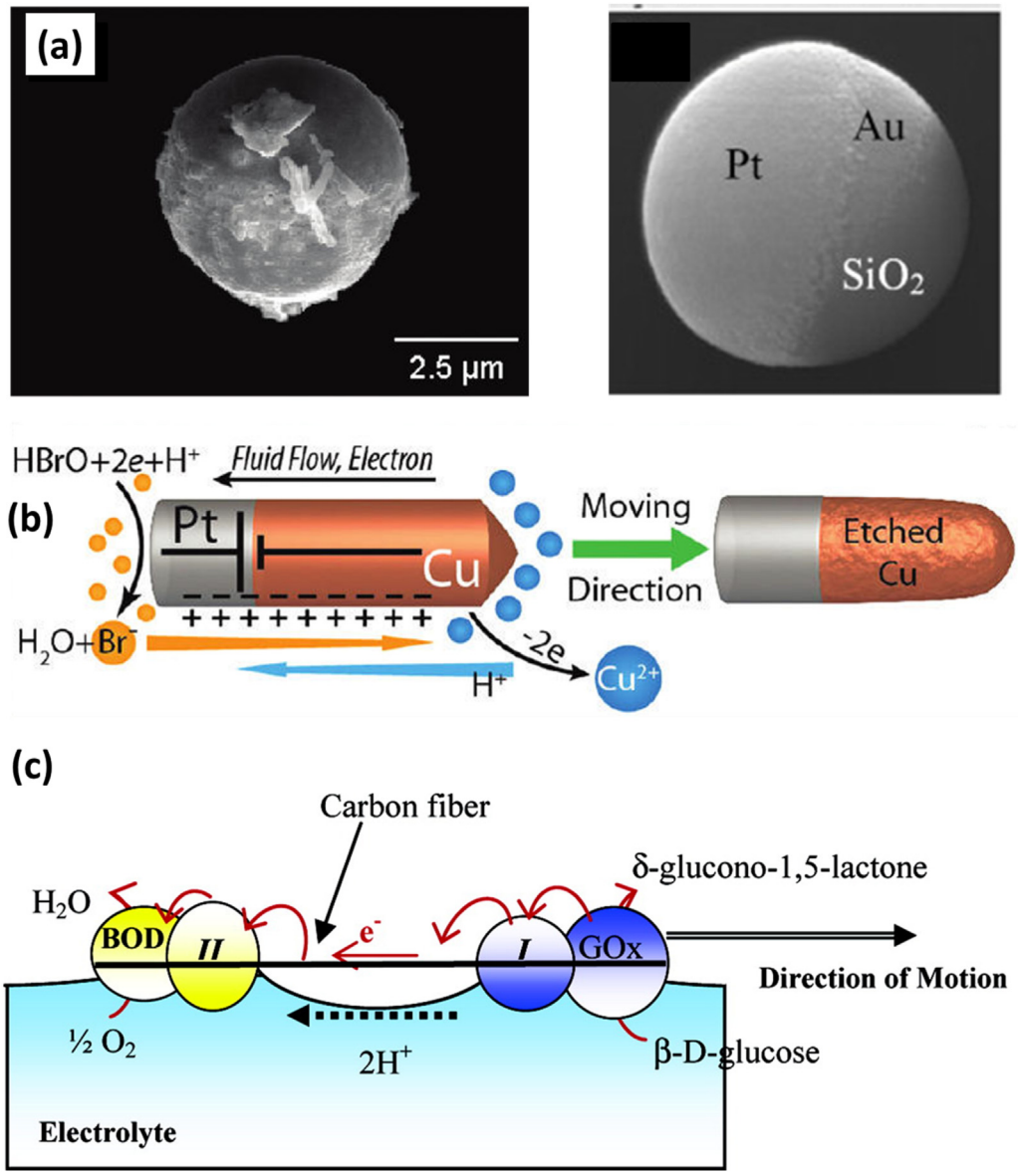

Figure 5 Examples of self-electrophoretic nano- and micromotors. (a) Janus bimetallic microspheres prepared by selective metal evaporation, from Ref. [53] (copyright 2010 The American Chemical Society, reprinted with permission) and [52] (copyright 2010 American Institute of Physics, reprinted with permission). (b) Cu—Pt motors operating in dilute Br_2 solutions [56], copyright 2011 The American Chemical Society. (c) Functionalized carbon fibers move at the air—water interface through self-electrophoresis [58], copyright 2005 The American Chemical Society, reprinted with permission.

These bimetallic nanorods were fabricated by template-assisted electrodeposition in anodized alumina oxide (AAO) membranes (Fig. 4c). The powered movement in these nanomotor systems immediately attracted attention in the scientific community because they were the first artificial microsystems to catalytically convert chemical energy to autonomous movement.

Following the discovery of the autonomously moving Au—Pt and Au—Ni nanorods, a research was carried out to understand the mechanism of catalytic energy conversion. A number of candidate mechanisms were proposed, including interface surface tension gradient, oxygen bubble recoil, and self-electrophoresis [7,30,46,47]. Experimental evidence and simulation results strongly suggested that self-electrophoresis is the dominant mechanism for catalytic motors on this length scale [30,48—51].

In self-electrophoresis, the charged microparticle moves in a self-generated electric field as a result of an asymmetric distribution of ions. For example in the case of the Au—Pt bimetallic nanomotors, the oxidation of H_2O_2 preferentially occurs at the anode (Pt) end and the reduction of H_2O_2 (and O_2) at the cathode (Au) end. This bipolar electrochemical reaction leads to a higher concentration of protons near the Pt end and a lower concentration near the Au end. Since the protons are positively charged, the asymmetric distribution results in an electric field pointing from the Pt end to the Au end. The negatively charged nanorod therefore moves in the electric field, an effect similar to electrophoresis.

Although a proton gradient is responsible for the motion of bimetallic motors in H_2O_2 solutions, other ions can also be used to propel motors by the same mechanism (discussed below). The key is an asymmetric distribution of ions that generates a local electric field.

Bimetallic, self-electrophoretic motors have also been studied in shapes other than rods. For example, Gibbs et al. fabricated spherical particles with overlapping Pt and Au regions by a dynamic shadowing growth technique [52] (Fig. 5, top left). The motion of the motors was studied by systematically varying exposed Au surface area. Wheat et al. fabricated electrophoretically active bimetallic spherical Janus particles by evaporating Au on half of a Pt coated microsphere [53] (Fig. 5, top right). They found that the motor speed increased linearly with increasing concentration of H_2O_2 between 0 and 1.5 mol/L. By further breaking the symmetry of the shapes of the motors, it is possible to introduce torque and therefore rotation of the motors. This was demonstrated first by Catchmark et al., who made gears of Au and Pt that rotated in H_2O_2 solutions [54]. Later Mirkin and co-workers and Wang et al. independently demonstrated the rotation of bi- and trimetallic nanorods by evaporating layers of different materials in non-cylindrical geometries [38,55].

Fuels other than H_2O_2 have also been shown to propel electrophoretically driven nano- and microscale motors. For example, Ibele et al. developed a micropumping system in which hydrazine (N_2H_4) and its derivative *asym-N,N*-dimethylhydrazine ($N_2Me_2H_2$) were used as fuels [31]. Optical tracking of tracer particles and mixed potential measurements on Au and Pt electrodes confirmed that hydrazine (and its derivatives) are preferentially oxidized or reduced on the electrode surface, leading to electrokinetic flows similar to those observed in H_2O_2 nanomotor systems. They also observed that the pumping direction could be switched by replacing N_2H_4 with $N_2Me_2H_2$, a result of the difference in the mixed potentials of Au and Pt in different fuels. Liu et al. demonstrated another bimetallic nanomotor system in which Cu—Pt nanorods (3—4 μm long and ~300 nm in diameter) move autonomously in dilute I_2 or Br_2 solutions at roughly 10 μm/s (Fig. 5, center) [56]. This Cu—Pt nanomotor system is more energy efficient than the Au—Pt nanorod motors mainly because there is minimal fuel waste on the catalytically active surface. Yoshizumi and coworkers developed spherical Zn—Pt Janus micromotors operating in Br_2, *p*-benzoquinone or methanol [57]. However the lifespan of both Cu—Pt and Zn—Pt motors are short due to the corrosion of the active metal segment of the wire. In another study, Mano and Heller reported that a piece of carbon fiber (7 μm in thickness and 0.5—1 cm in length) was able to move at air—water interface at 1—0.1 cm/s for 3 min before stopping (Fig. 5, bottom) [58]. The propulsion was attributed to a bioelectrochemical reaction:

$$\beta\text{-D-glucose} + \frac{1}{2}O_2 \rightarrow \delta\text{-glucono-1, 5-lactone} + H_2O \qquad (3)$$

with half reactions occurring at the anode functionalized with glucose oxidase and cathode functionalized with bilirubin oxidase, respectively. The proton gradients formed by the half reactions are ultimately responsible for the motion through the self-electrophoresis mechanism. This glucose driven motor system holds promise for use in biological systems because it uses bio-available fuels: glucose and oxygen. However, its ability to move only at the air—water interface and at high oxygen pressure for a short time presents challenges for use in real biomedical or bioanalytical applications.

Much effort has been devoted to improving bimetallic nanomotors propelled by self-electrophoresis, mainly to achieve faster speeds. Zacharia et al. discovered that the speed of bimetallic nanomotors can be increased by increasing their catalytic surface area [59]. A series of reports from the Wang group described bimetallic nanomotors modified in various ways, reaching a speed of ~100—200 μm/s [60,61]. In one report Ag—Pt nanorods were synthesized and showed autonomous motion at speed as high as 40 μm/s [62]. When an Ag—Au alloy was used as the cathode material instead of Au, it was discovered that the speed of the nanomotors increased to 150 μm/s [63]. Carbon nanotubes have also been incorporated into the Pt segment during the electrodeposition step, and the resulting motors reach a speed of 50—60 μm/s [64]. By using a mixed fuel of H_2O_2 and hydrazine, the motor speed further increased to 94 μm/s. The dramatic increase in motor speed in these cases can be attributed to a larger mixed potential difference between the two electrodes, which was determined by Wang et al. to be a critical parameter affecting the motor speed [49].

Another important aspect of the research on self-electrophoretically driven nanomotors is the development of other functionalities, such as pumping, rotation, directionality and speed control, sensing capabilities, and cargo pick up and delivery. Here we briefly summarize the major progress made in this field in Table 1. Review articles have been published on specialized topics in this area including transport and delivery of cargo [65,66] and sensing [67].

Although significant progress has been made in research on self-electrophoretically propelled nano- and microscale motors, there exist a few issues that must be addressed in order to expand their applications, especially in biologically relevant media. First, most electrophoretically driven nano- and microscale motors rely on toxic fuels such as H_2O_2 or hydrazine. As noted earlier, there has been research to replace these toxic fuels with more biocompatible chemicals such as glucose [58]. However significant improvements in efficiency are needed for such motor systems to be able to move in biological fluids at low glucose and oxygen concentration. Other possibilities such as Br_2, I_2 or methanol have been proposed, but glucose remains the most promising one. Even if appropriate fuels were found, one still needs to overcome the problem that self-electrophoresis does not work at high ionic strength, as has been shown both theoretically and experimentally [30]. Although these motors can tolerate a low concentration of ionic solutes (*e.g.*, up to 10^{-4} mol/L of Ag(I) ion) [79], the limited activity of electrophoretically driven nanomotors does not bode well for use in biological media of high ionic strength (~0.2 mol/L for blood serum). Finally, self-electrophoretically driven nanomotors have an extremely low energy efficiency, on the order of 10^{-8}—10^{-9} (discussed in more detail in later section) [47,81]. New fuels, motor designs, and propulsion schemes are needed to improve the energy efficiency to the point where fast and powerful nanomotors can operate at low fuel concentrations.

Table 1 Summary of modifications and applications of self-electrophoretic nanomotors.

Functionality	Ref.	Description	Note
Speed control	[68]	Nanomotor speed can be tuned by sweeping the electrical potential of gold wire electrode close to the wires.	Interfacial tension gradient at different oxygen concentrations at different electrochemical potentials was used to explain the motor speed change.
	[69]	Heat pulse is used to increase the speed of bimetallic nanomotors to 45 μm/s at 65 °C	The increase of motor speed was attributed to faster electrochemical reactions and lower fluid viscosity at elevated temperatures.
Direction control	[70]	Ni segment was incorporated into bimetallic nanomotors and external magnetic field was used to guide the motion.	Due to the low speed, Brownian motion was still significant and the controllability was therefore slightly compromised.
	[71]	Silver-Dynabead doublet nanomotors respond to magnetic field and align.	Although chaining and swarming were demonstrated, individual control of the doublet with magnetic field was difficult.
	[72]	Catalytic Au—Pt nanorods were shown to be guided by the domain boundary structure on a thin magnetic garnet film.	
	[73]	The direction of Pt—Au—Ag_{flex}—Ni four segment nanorods could be switched by activating magnetic rotation of the tail.	Although the self-electrophoretic part of the motor becomes inactive at high salt concentration, the propulsion is salt concentration independent.
	[74]	Au/Ni/Au/Pt—CNT nanomotor was synthesized and its motion could be guided in microchannels by external magnets.	Cargo manipulation was also demonstrated.
Pumping	[27,48]	Pumping of fluid and tracer particles by bimetallic ring and disk structures was demonstrated.	Depending on the zeta potential of the particle and the bottom substrate, the direction of particle motion can be reversed.
	[29]	A biomimetic pump was fabricated by evaporating Au and Pt on each side of a polycarbonate membrane. When the membrane is placed in 0.01 wt% H_2O_2 solution it had a pumping rate of 3 nL/(μA s).	When two electrodes are connected the pump operates by taking advantage of the same electrokinetic phenomenon what powers bimetallic nanomotors, only in the form of electroosmosis.
Rotation	[39]	Au—Ni nanorods (~2.5 μm long and 300 nm in diameter) were seen to move and rotate autonomously in H_2O_2 solutions.	Two modes of rotation were observed: tethered rotation near an impurity site on the Si substrate, and orbiting around the center as a result of the asymmetric shape of the nanorod.
	[54]	Rotating gears (~150 μm in diameter) were fabricated through photolithography with Pt deposited on the teeth of a Au gear. The gears rotated at ~60 rpm in ~1% H_2O_2 solution.	The gear rotates by the same electrophoretic mechanism that propels bimetallic nanomotors. The direction of the rotation also agrees well with the mechanism.
	[38]	A thin layer of gold was evaporated on Au—Pt nanomotor. At a length ratio of Pt/Au of 2, the nanorod (360 nm in diameter, 5 μm in length) rotated at ~20 rpm in 3% H_2O_2.	The decomposition of H_2O_2 into O_2 on the surface of the asymmetrically shaped nanorods was proposed to explain the rotation.
	[26]	A nanorotor was fabricated by evaporating Cr/SiO_2/Cr, Au and Pt on one side of Au—Ru nanomotors. The nanorods rotated at an average rate of 180 rpm in 15% H_2O_2 solution.	The rotation of the nanorod was attributed to a vector sum of self-electrophoretic forces in two directions. Interesting dynamic interactions were also observed for these rotors but not explained in depth. The direction of rotation was not easily distinguishable due to low optical resolution.
Cargo towing and delivery	[75]	Au—Ni nanorods were synthesized and upon magnetic activation could couple particles and move at ~10 μm/s.	The cargo towing of these nanomotors was attributed to the hydrodynamic interactions between the rotating Ni tail and the particle being carried.

Table 1 (*Continued*)

Functionality	Ref.	Description	Note
	[76]	Cargo-towing on bimetallic nanomotors was enabled by either electrostatic attachment or biotin-streptavidin binding.	Speed of the motor with cargos attached decreases with increasing cargo sizes.
	[77]	Cargo attached on bimetallic nanomotors can be released by UV light through either dissolving one metal segment or linker photolysis.	Cargo drop-off by metal dissolution takes 10—20 s, while photolysis of linkers takes 60—100 s.
	[78]	Catalytic nanomotors were demonstrated to pick up, transport and release PLGA particles and liposomes.	The iron-oxide encapsulated PLGA particles attached to the Ni segment in the nanomotor through magnetic interaction. Release of cargo was accomplished by the fast reversal of the motor direction. Motor speed decreases with increasing cargo size.
Sensing	[79]	Ag(I) ion in water (0.5—100 μM) can trigger an increase of the speed of catalytic bimetallic nanomotors, thus enabling motion-based sensing.	Under-potential deposition of silver on Au—Pt nanomotors, and the consequent change in surface properties, was proposed as the leading mechanism for the acceleration of nanomotors in the presence of silver ions.
	[80]	The acceleration of catalytic nanomotors in the presence of silver ions was exploited in detecting DNA and bacterial ribosomal RNA down to the 40 attomole level.	DNA assay was tagged with silver nanoparticles and the release of silver ions induced nanomotor acceleration.

Self-diffusiophoresis

Diffusiophoresis is a phenomenon in which the motion of particles is driven by a concentration gradient of solutes [82]. Diffusiophoresis can be classified into two categories: electrolyte and nonelectrolyte diffusiophoresis, in which the molecules contributing to the gradient are charged or uncharged, respectively. Chemical reactions taking place at surfaces consume reactants and generate products, leading to concentration gradients that in turn power the motion of synthetic motors and pumps. In these cases, the term *self-diffusiophoresis* has been suggested as the propulsion mechanism due to the fact that the concentration gradient is generated by the motor particles themselves.

Electrolyte diffusiophoresis, which is the more commonly exploited in nano- and micromotors and pumps, was first experimentally demonstrated by Ebel et al. [83]. For a concentration gradient ∇c of monovalent salt, the velocity $\mathbf{U}$ of a charged particle near the charged surface is governed by the following equation [84]:

$$\mathbf{U} = \underbrace{\frac{\nabla c}{c_0}\left[\left(\frac{D^+ - D^-}{D^+ + D^-}\right)\left(\frac{k_B T}{e}\right)\frac{\varepsilon(\zeta_p - \zeta_w)}{\eta}\right]}_{\text{Electrophoretic term}} + \underbrace{\frac{\nabla c}{c_0}\left[\left(\frac{2\varepsilon k_B^2 T^2}{\eta e^2}\right)\{\ln(1-\gamma_w^2) - \ln(1-\gamma_p^2)\}\right]}_{\text{Chemophoretic term}} \quad (4)$$

where D^+ and D^- are the diffusion coefficients of the cation and anion respectively, c_0 is the bulk concentration of ions, e is the charge of an electron, k_B is the Boltzmann constant, T is the absolute temperature, ε is the dielectric permittivity of the solution, η is the viscosity, ζ_p and ζ_w are the zeta potentials of the particle and wall, respectively, and $\gamma_f = \tanh(e\zeta_f / 4k_B T)$.

Fig. 6 shows a generic scheme of electrolyte diffusiophoresis, in which a charged particle is driven by a concentration gradient of ionic species. Because the cations and anions diffuse at different rates, an electric field arises that can propel a charged particle (the electrophoretic term in Eq. (4)). In addition, cations and anions interact with the double layer of the charged particle differently, resulting in a pressure that moves the particle (the chemophoretic term in Eq. (4)). In most cases, chemophoretic effects are negligible and the directions of diffusiophoretic flows are governed by the electrophoretic effect, unless the diffusivities of the cations and anions are very similar.

Particle motion is often further complicated by the presence of a charged substrate, where electroosmotic flow can also occur. Depending on the relative magnitudes of the surface charges on the particle and the substrate, the competition between electrophoretic diffusiophoresis and electroosmosis can result in particle motion in either direction, as has been shown experimentally [85,25,86].

The most effective nano- and micromotor and pumps that are powered by electrolyte self-diffusiophoresis rely on gradients of H^+ or OH^- ions, taking advantage of their fast diffusion and therefore significant contribution to the electrophoretic term in the diffusiophoresis equation. The first micromotors propelled in this way were light-triggered silver chloride particles reported by Ibele et al. (Fig. 7, top) [25]. In UV light, silver chloride particles react with water to produce protons, chloride ions, and hypochlorous acid at their surfaces. Since protons diffuse much faster than chloride ions ($D_H = 9.311 \times 10^{-5}\ cm^2\ s^{-1}$,

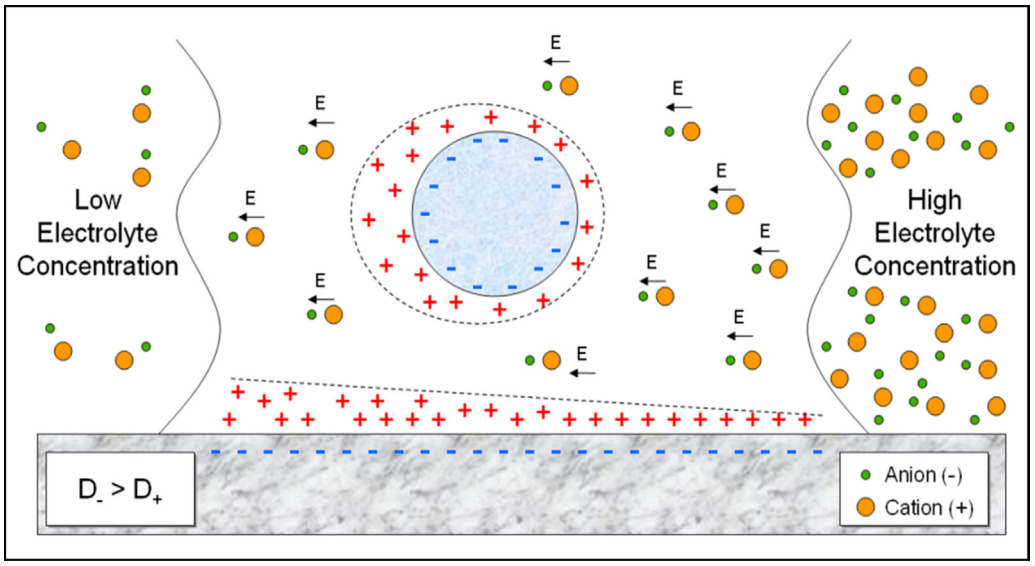

Figure 6 Scheme of electrolyte diffusiophoresis of a negatively charged particle near a negatively charged surface.

$D_{Cl-} = 1.385 \times 10^{-5}$ cm^2 s^{-1} at 298 K), inward electrical fields (E) are generated, resulting in electrophoresis of the particles and electroosmosis along the wall. Since the particles are irregularly shaped, the symmetry of the electrolyte concentration gradient around particles is broken, and unbalanced local electrical fields drive the directional movement of the charged particles at velocities on the order of 1–10 μm/s. Later examples of self-diffusiophoretic micromotors have followed essentially the same principle [32,71,84–87]. Electrolyte diffusiophoresis can also lead to the emergence of collective behavior, in which motor particles can communicate with each other and work cooperatively to form dynamic structures. This effect is discussed in more detail below.

Electrolyte diffusiophoresis can also drive the pumping of fluid or particles, which can be initiated by light [34] or chemicals [27,28,30,31,88]. An example of such a system is shown at the bottom of Fig. 7 [34]. UV light decomposes a photoacid generator (PAG) into fast protons and slower anions, which leads to an inward electrical field. The field drives charged tracer particles toward or away from the PAG by the combination of electrophoresis and electroosmosis.

Concentration gradients of neutral species (non-electrolytes) can also induce motion. Although the forces generated are generally lower than with electrolyte diffusiophoresis, neutral solute gradients can be effective for propulsion even in solutions of high ionic strength. One such propulsion mechanism is non-electrolyte diffusiophoresis, although others (such as osmophoresis and density gradients) are possible as well. In non-electrolyte diffusiophoresis, the force arises from steric exclusion generated by the solutes interacting with the particle surface, which creates a pressure gradient along the particle [33]. Asymmetry in particle composition, morphology, or reaction rate leads to an asymmetric distribution of chemical species, which breaks the symmetry of the pressure distribution and

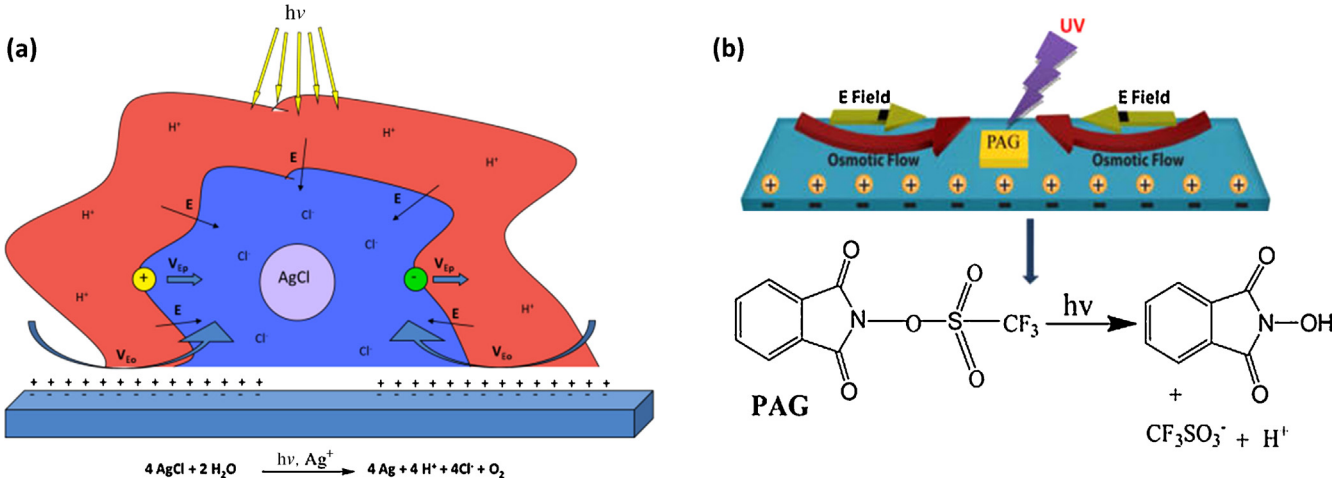

Figure 7 (a) Schematic drawing of electrolyte self-diffusiophoresis of silver chloride microparticles in response to UV light [89]. Reproduced with permission from The Royal Society of Chemistry. (b) Design of electrolyte self-diffusiophoretic pumps based on the light-initiated decomposition of a PAG [34]. Copyright 2012 The American Chemical Society, reprinted with permission.

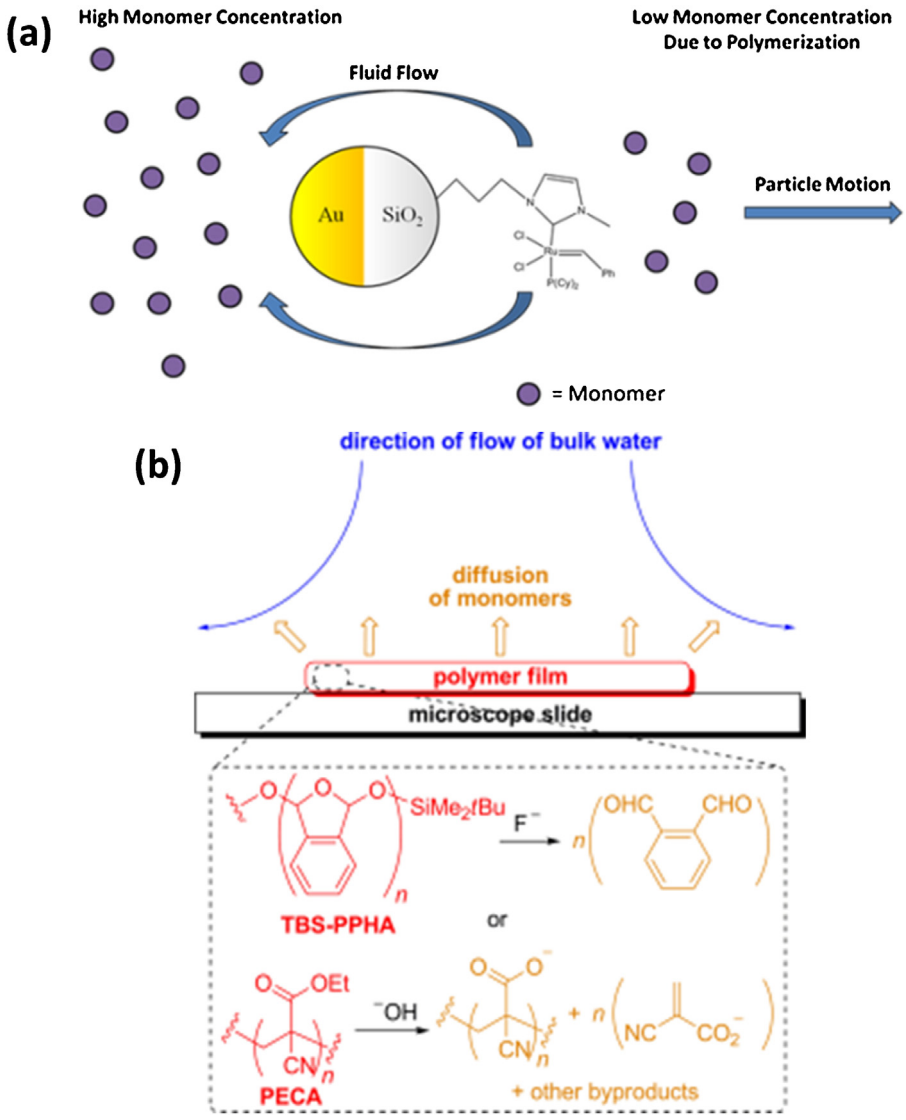

Figure 8 (a) Illustration of non-electrolyte diffusiophoresis in polymerization-powered micromotors [93]. Fluid flows from the low to high solute concentration side of the particles, and the motor moves in the opposite direction. Copyright 2011 John Wiley & Sons, Inc., reprinted with permission. (b) Design of non-electrolyte diffusiophoretic micropumps based on analyte-induced depolymerization of a polymer film [33]. A concentration gradient of the depolymerization products leads to outward fluid flow, which carries tracer particles. Copyright 2012 John Wiley & Sons, Inc., reprinted with permission.

leads to directional motion of particles. Theoretical studies have suggested that microparticles can be propelled by non-electrolyte diffusiophoresis by generating a chemical gradient of uncharged species [90,91]. The movement of particles down non-electrolyte static concentration gradients has also been experimentally demonstrated by Staffeld and Quinn [92].

Pavlick et al. have observed the autonomous movement of particles propelled in catalytically generated non-electrolyte concentration gradients [93] (Fig. 8 top). In this system, a Grubbs olefin metathesis catalyst bound to a 1 μm Au-silica Janus sphere catalyzes the polymerization of norbornene. Although no directional movement was observed for these particles, a significant increase in the diffusion coefficient was observed [94]. The inverse of this motor system has also been explored, where one side of the particle creates more reactants than products [33,95,96]. Microscale pumps can be designed to operate by non-electrolyte diffusiophoresis as well, and they are usually a more sensitive indicator of the weak flows generated than autonomously moving particles. In one example reported by Zhang et al., a depolymerization reaction at the surface of a polymer film produces gradients of monomers that drive the fluid away from the pumps. Tracer particles (*e.g.* PS-NH_2, PS-COOH, *etc.*) are therefore pumped away from the surface, regardless of their surface charges (Fig. 8, bottom). Pumping speeds vary with reaction rate and distance from the pump, and are on the order of 1—10 μm/s [33].

Self-acoustophoresis

Because one of the strong drivers of nanomotor research is their potential utility in biomedicine and diagnostics

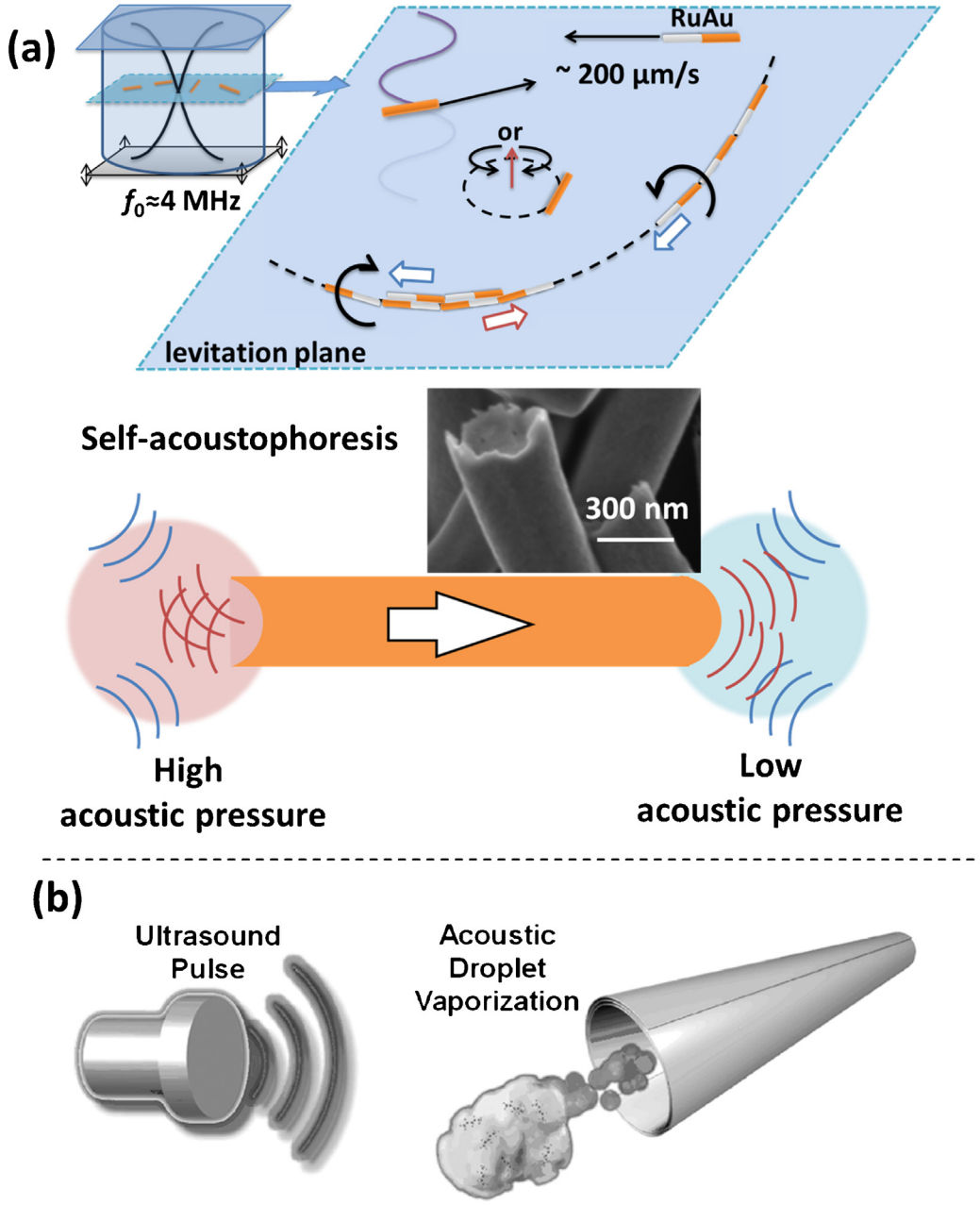

Figure 9 Ultrasonically propelled micromotors. (a) Asymmetrically shaped metallic microrods are activated in an ultrasonic standing wave at MHz frequency through a self-acoustophoresis mechanism [36], copyright 2012 The American Chemical Society, reprinted with permission. (b) Bubble recoil propels metallic microtubes when an ultrasound pulse vaporizes a droplet of perfluorocarbon fluid [106], copyright 2012 John Wiley & Sons, Inc., reprinted with permission.

[97,98], there is a need to develop propulsion mechanisms that can operate in biocompatible media, including *in vivo*. Two serious drawbacks of chemical propulsion schemes are their reliance on toxic fuels such as H_2O_2 [7,84], hydrazine [25,31,64] and halogens [56,57], and their intolerance of media that contain salts. Although nano- and micromotors can be driven by external fields [16,18—22,99], as noted above such motors are usually not autonomous. Thus there is a need for new propulsion mechanisms that can generate autonomous movement in biological media.

Ultrasonic energy is promising for propelling nano- and micromotors. Low power acoustic waves are safe and are used extensively for *in vivo* imaging [100,101]. Research on ultrasonic manipulation of microparticles dates back to the 19th century [102], and there is a vast literature on the topic, especially in the field of microfluidics [103,104]. In an acoustic field, suspended microparticles experience acoustic radiation forces and move to the pressure nodes (or antinodes) as a result of pressure gradients. When the acoustic excitation meets the criteria to form standing waves, the radiation force is the strongest and can be expressed as [105]:

$$F_{ax} = 4\pi a^3 E_{ac} k \sin(2kz)\Phi \quad (5)$$

where F_{ax} is the acoustic radiation force, a is the particle radius, E_{ac} is the acoustic energy density, k is the wavenumber, z is the distance of the particle from the node, and Φ is the acoustic contrast factor which can be expressed as:

$$\Phi = \frac{\rho_p + (2/3)(\rho_p - \rho_0)}{2\rho_p + \rho_0} - \frac{1}{3}\frac{\rho_0 c_0^2}{\rho_p c_p^2} \quad (6)$$

here ρ_p and ρ_0 are the density of the particle and medium, respectively, and c_p and c_0 are the speed of sound in the particle and surrounding medium, respectively. Acoustic radiation forces are the basis of ultrasonic particle manipulation techniques. However most studies of this effect have focused on symmetric particles, typically of soft polymer or biological materials such as polystyrene spheres or cells.

In 2012 we reported the first autonomous micromotors propelled by MHz frequency ultrasound [36] (Fig. 9, top panel). In this system, metallic microrods are suspended in water in an acoustic chamber. A vertical standing waves levitates the particles to a plane at the midpoint of the cell where the pressure is a minimum. In that plane the metal microrods exhibit axial motion at speeds up to 200 μm/s in water. The particles also form patterns in the nodal plane as a result of nodes and anti-nodes within the plane. The composition of the microrods was found to significantly affect their movement, with only metal microparticles showing fast axial motion.

Although the forces responsible for acoustic propulsion of metallic microrods are not completely understood, the leading candidate is a mechanism called self-acoustophoresis. This mechanism was built on the observation that the microrods fabricated always had concave ends. Thus the strong axial propulsion of these metallic nanorods has been proposed to originate from the differential scattering of acoustic waves at the ends of the rods. Asymmetric scattering of acoustic waves leads to a pressure gradient that is high at the concave end and low at the convex end, with a difference of *ca.* 1 Pa. Through an estimate of the forces at play in this system, it was further determined that the scattered sound waves are traveling in the z direction, rather than propagating in the x–y plane (the plane in which the motors travel). The forces imparted by the latter are about two orders of magnitude lower than the axial propulsion force.

In addition to self-acoustophoresis, Wang and coworkers have recently shown that ultrasonic energy can power micromotors by bubble propulsion [106] (Fig. 9, bottom panel). In this system metallic microtubes that contain trapped perfluorocarbon (PFC) are propelled axially by the ejection of PFC bubbles. These motors (tens of μm in length) can reach an impressive speed of 6.3 m/s, and are powerful enough to penetrate deep into lamb kidney tissues. The speed and power of these ultrasonic microtubular motors can be modulated by the pulse length and amplitude of the ultrasound.

A number of issues remain to be addressed for acoustic motors to be useful in biomedical applications. Bubble-propelled motors, despite their high power and speed, currently rely on a finite supply of fuel and hence can operate for only a short time. Their relatively large size (a minimum size of 8 μm was proposed) limits their use *in vivo*, where large particles are rapidly cleared [107,108]. Self-acoustophoretic metal nanorods are similar in size to bacteria and are likely to be cleared less rapidly, but they have lower power and speed, as well as the requirement of an acoustic standing wave. Needlessly to say, significant research is required for either ultrasonic micromotor system to become competent for biomedical tasks.

Self-thermophoresis

Gradients of temperature, just like gradients of chemical concentration, electric potential, and acoustically generated pressure, can also induce motion of colloidal particles. This is called thermophoresis, or the Soret effect, and has been known and studied for over 150 years [109]. However the study of thermophoresis has been mostly carried out in macroscopic systems in which colloidal particles collectively migrate in an externally established thermal gradient.

Recently, microswimmers propelled by self-generated temperature gradients have been studied [110–112]. Jiang et al. in 2010 demonstrated self-thermophoresis at the single particle level (see Fig. 10, top) [110]. Janus silica microspheres half-coated with Au were irradiated in water with a defocused laser beam at 1064 nm. Absorption of light by the thin gold layer produced heat, which generated a local temperature gradient (~2 K across the particle) and induced thermophoresis. Later, Baraban et al. used an AC magnetic field to heat Permalloy-capped silica particles in solution and observed autonomous propulsion [111] (Fig. 10, bottom). The temperature difference across the particle was estimated to be 1.7 K. More recently Qian et al. have used laser light to ''nudge'' gold-capped polystyrene microspheres [112]. They adopted a ''Maxwell demon'' approach using real time location monitoring and applying power only when the particle was facing in the desired direction. A temperature different across the particle of ~7 K was obtained, and thermophoresis as well as photon momentum transfer were considered to contribute to the motion. Although the term ''photophoresis'' was used to attribute to the thermal contribution, it can also be categorized as self-thermophoresis. In all three cases, the micromotors moved away from the heated side of the particle, exhibiting positive Soret effect. Later Golestanian studied the collective behaviors of self-thermophoretic micromotors using a stochastic formulation [113]. He found that thermorepulsive motors could organize into different structures while thermoattractive motors became unstable. Through numerical modeling, Yang and Ripoll demonstrated that the self-thermophoresis mechanism is also applicable to nanodimers [114].

Other mechanisms

Here we briefly introduce a few important kinds of nano- and micromotors that are driven by mechanisms other than self-generated fields. Although these are beyond the scope of this review, they constitute an important area in nano- and micromotor research and hold considerable promise in the future development of this field.

Bubble-propelled microspheres and microtubes are powered by chemical species (typically H_2O_2) that react on the surface of the motor to generate bubbles. Detachment of the bubbles propels the motors through a recoil force (see Fig. 11) [6,35,115]. These motors, which range in size from a

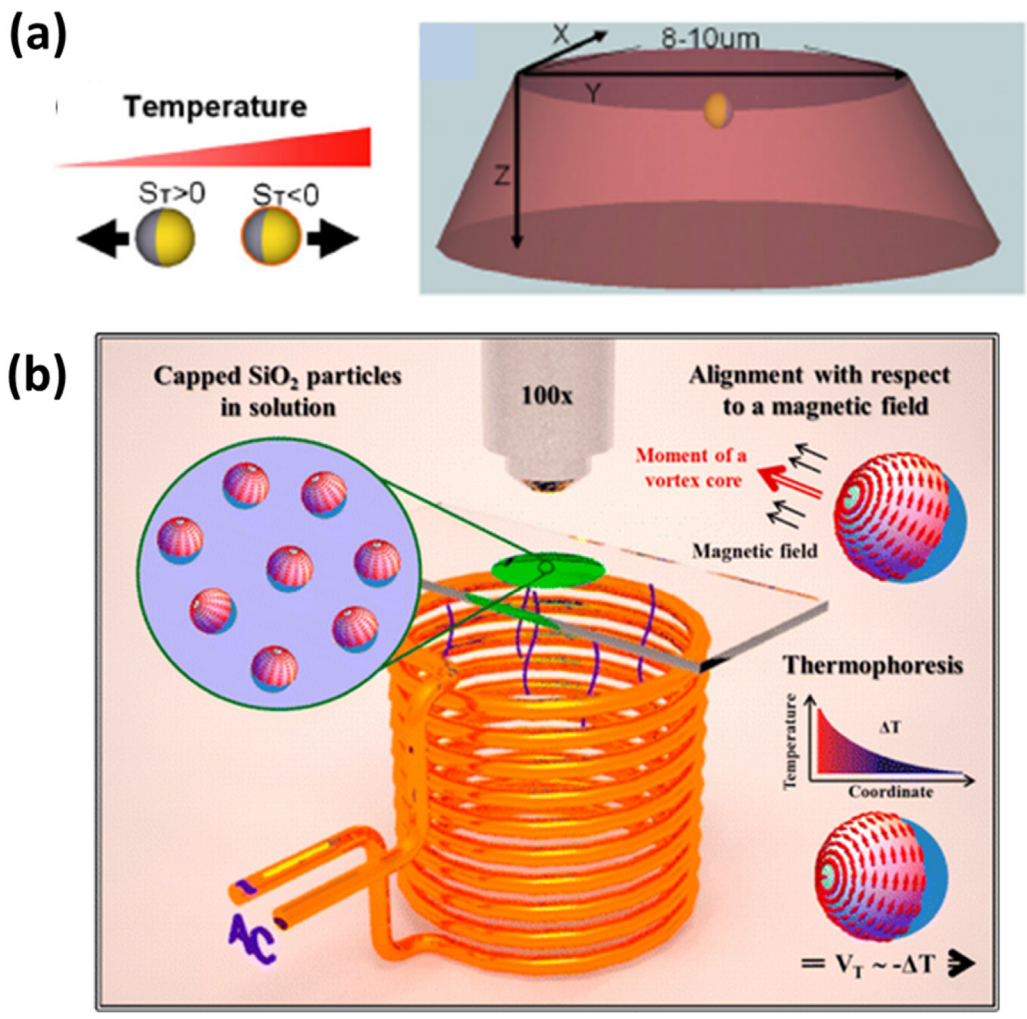

Figure 10 Self-thermophoretic microparticles. (a) Gold capped silica microspheres undergoing autonomous motion due to the Soret effect in a defocused laser beam [110], copyright 2010 The American Physical Society, reprinted with permission. (b) Permalloy-capped silica particles move by self-thermophoresis in an AC magnetic field [111], copyright 2012 The American Chemical Society, reprinted with permission.

few micrometers to hundreds of micrometers, can be quite fast and powerful, and a number of interesting functionalities have been demonstrated including cargo delivery, sensing and tissue penetration [116,117]. Although there has been no comprehensive review of this motor type, readers are directed to a few review articles [61,118,119].

External fields can also be used to propel nano- and microscale motors. Examples (see Fig. 12) include millimeter size diodes that move in AC fields through self-electroosmosis induced by a rectifying junction [99,16] (Fig. 12a), particles moving in DC electric fields through surface bipolar electrochemical reactions [18,120] (Fig. 12b), and magnetic microparticles propelled by body rotation or deformation [19—22] (Fig. 12c—e). A few review papers touch upon these topics and are recommended for interested readers [121—123].

Energy conversion efficiency

Although the figure of merit in characterizing and comparing different nano- and micromotors is typically speed or force, their energy efficiency is an equally important parameter that deserves proper attention. Designing nano- and micromotors of higher energy efficiency can enable applications that involve on-board fuel, or fuel present at low concentration in the environment, such as glucose/oxygen. Biological motors, for example, meet these requirements because of their high efficiency.

Few literature reports discuss the topic of the energy efficiency, defined as the mechanical power output divided by the overall energy input, in the field of nano- and micromotors [47,64,124—127]. Nevertheless, one general conclusion can be safely drawn: the efficiency of such these motors is typically orders of magnitude lower than their macroscopic counterparts (*e.g.*, common electric motors have energy efficiency close to 1) or biological motor proteins (*e.g.*, kinesin has an energy efficiencies of about 60% [128,129]). For example bimetallic Au—Pt nanomotors propelled by self-electrophoresis were found to have energy efficiency on the order of 10^{-9} [47]. We have identified four stages of energy loss that explain the low energy efficiency of self-electrophoretic catalytic micromotors. They

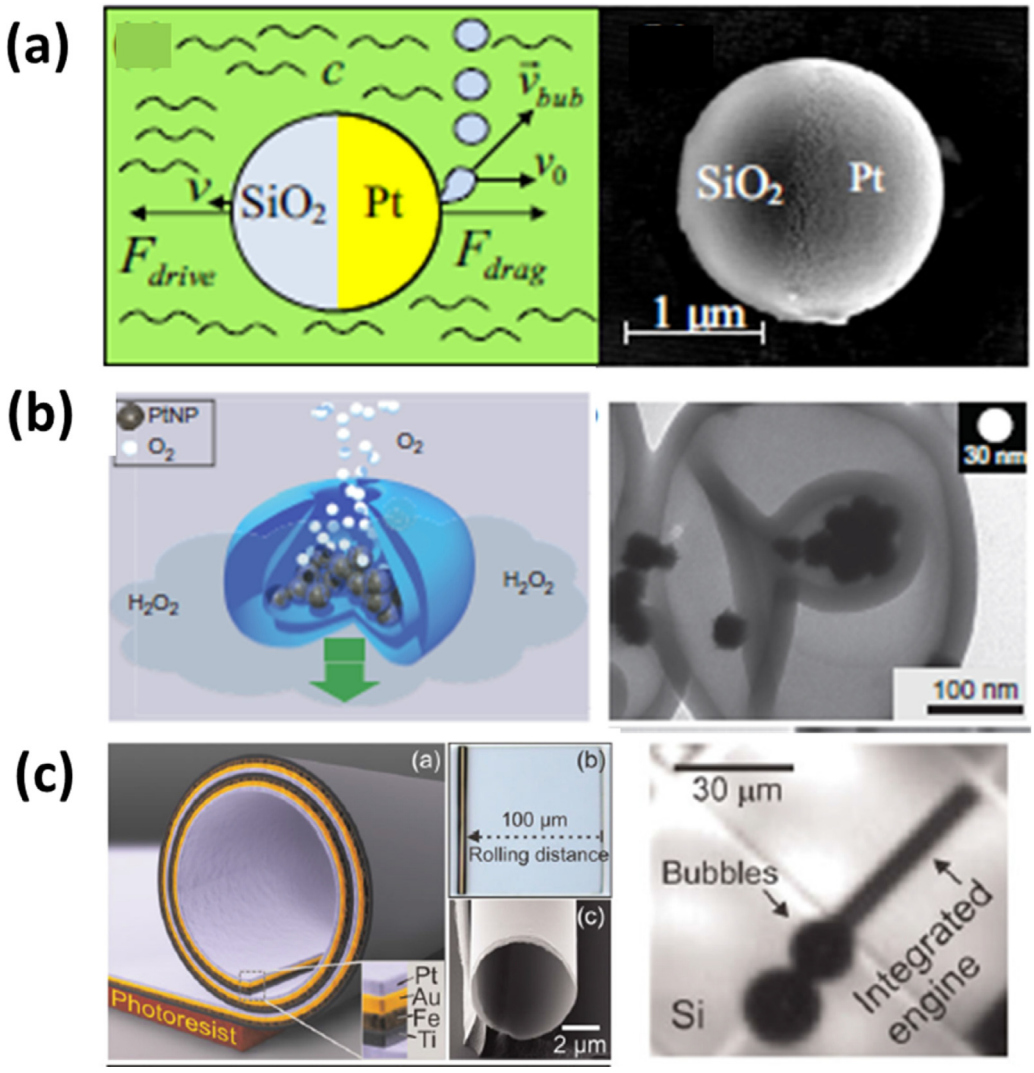

Figure 11 Examples of bubble propelled micromotors. (a) Janus Pt—SiO_2 spheres moving in H_2O_2 [35], copyright 2009 American Institute of Physics, reprinted with permission; (b) polymer capsules loaded with Pt nanoparticles moving in H_2O_2 [115], copyright 2012 Nature Publish Group, reprinted with permission; (c) rolled-up microtubes jetting through H_2O_2 solution [6], copyright 2009 John Wiley & Sons, Inc., reprinted with permission.

are the non-electrochemical consumption of fuel on the catalytic surface, the low efficiency of converting reaction free energy to an electric potential gradient along the motor surface, the low efficiency of converting the electric potential difference to mechanical work, and reverse electroosmotic flow over the charged substrate [81]. Together these four stages account for 9—10 orders of magnitude of energy loss, which agrees well with previous estimates of the overall efficiency. The energy efficiency of bubble propelled micromotors and helical magnetic motors were also estimated and found to be on the order of 10^{-10} and 10^{-3}, respectively. The approximate efficiency of different kinds of motors, including some macroscopic motors, is plotted in Fig. 13.

The low efficiency of self-electrophoresis as a propulsion mechanism is a common feature of many motor systems driven by self-generated chemical gradients. In other words, phoretic motors responding to self-generated fields are intrinsically inefficient, a conclusion shared by a number of theoretical studies of nano- and micromotors propelled by self-generated chemical gradients [124—127]. For example, Sabass and Seifer discovered that the overall energy efficiency of a self-diffusiophoretic nano- or micromotor was dependent on a number of parameters, such as the reaction rate, the diffusion coefficients and particle size [125]. For diffusiophoretic motors around 1 μm in size they estimated the efficiency to be on the order of 10^{-9}. The hydrodynamic efficiency (defined as mechanical power output divided by hydrodynamic power input) is specific to the propulsion mechanism but is independent of how fast the chemical species are produced or diffuse. It is on the order of 10^{-3} for motors of interest in this review (between 100 nm to a few μm) [127]. This agrees well with our estimate of the propulsion efficiency of self-electrophoretic motors [81].

The size of motors is an important parameter in determining their speed and efficiency, and theoretical studies suggest that the efficiency of diffusiophoretic motors should

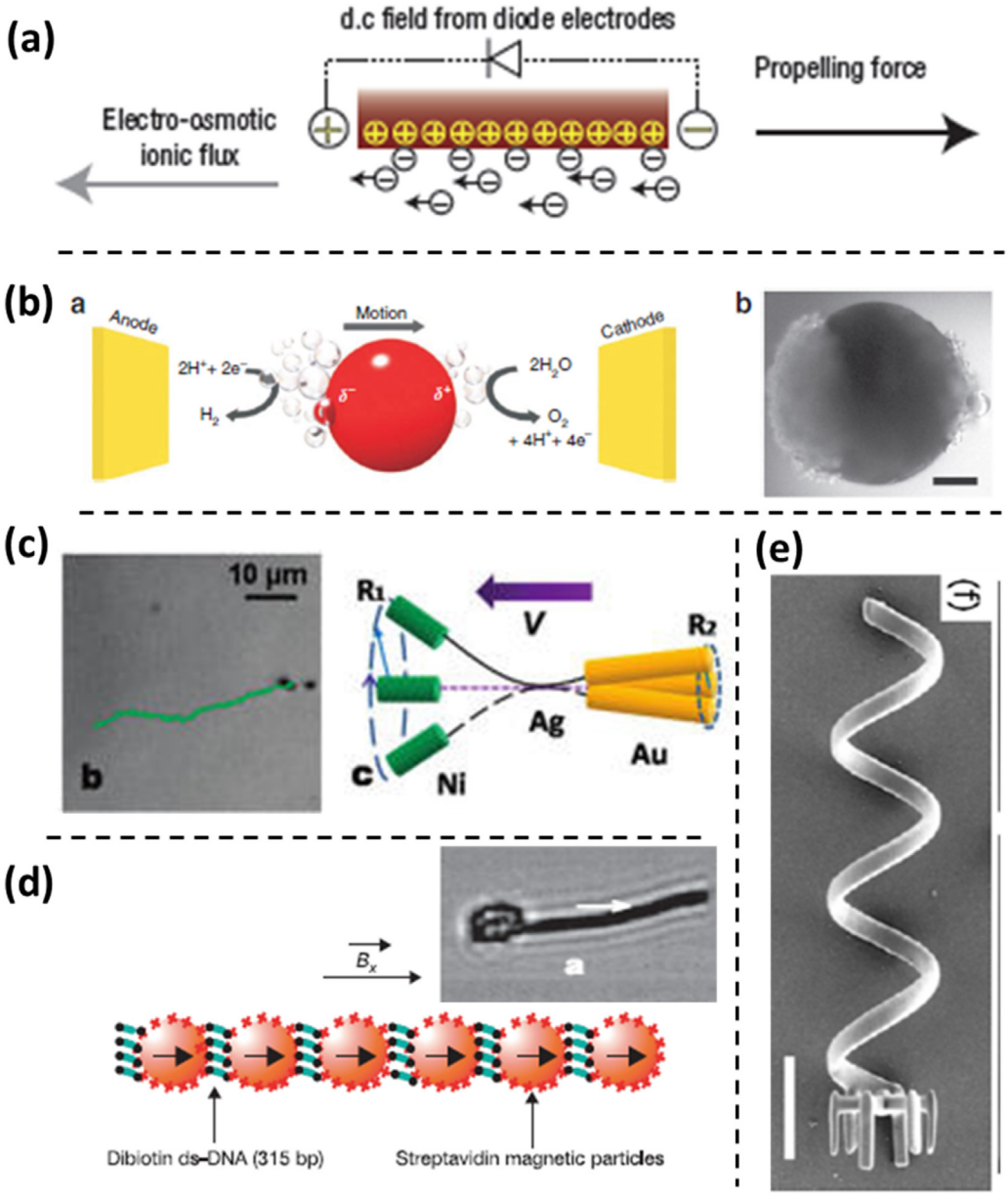

Figure 12 Examples of nano- and micromotors driven by external fields. (a) AC field driven diode motors [99,16], copyright 2007 Nature Publishing Group, reprinted with permission; (b) conductive microspheres by bipolar electrochemical reactions [18], copyright 2011 Nature Publishing Group, reprinted with permission; (c—e) magnetic field-driven micromotors [19,20,22], copyright 2005 Nature Publishing Group, reprinted with permission, 2010 The American Chemical Society, 2012 John Wiley & Sons, Inc., reprinted with permission.

scale inversely with their size [125,127]. The idea of scaling phoretic motors to tens or hundreds of nanometers is interesting and is precedented by studies of powered diffusion of enzymes such as urease [131]. However, the powered motion of nanomotors is complicated by Brownian motion that is dominant at such scales. In general, biological motors that operate on the nanoscale overcome this problem by confinement to a membrane or linear polymer, such as RNA or a microtubule. Learning from the mechanisms used by biological motors, including Brownian ratchets, may prove to be critical for the development of motors at sizes of hundreds of nanometers and below.

Collective behavior

Because the motors described above are powered by chemical gradients, they respond to each other when their self-generated gradients overlap, and they are also sensitive to externally applied gradients and fields. One of the most interesting and potentially useful emergent behaviors of autonomous motors is chemotaxis, the preferential movement in a direction defined by a chemical signal. Chemotaxis has long been known in biological systems [132], and recently has been observed in a few artificial systems and enzymes *in vitro* as well [93,133,134], although the

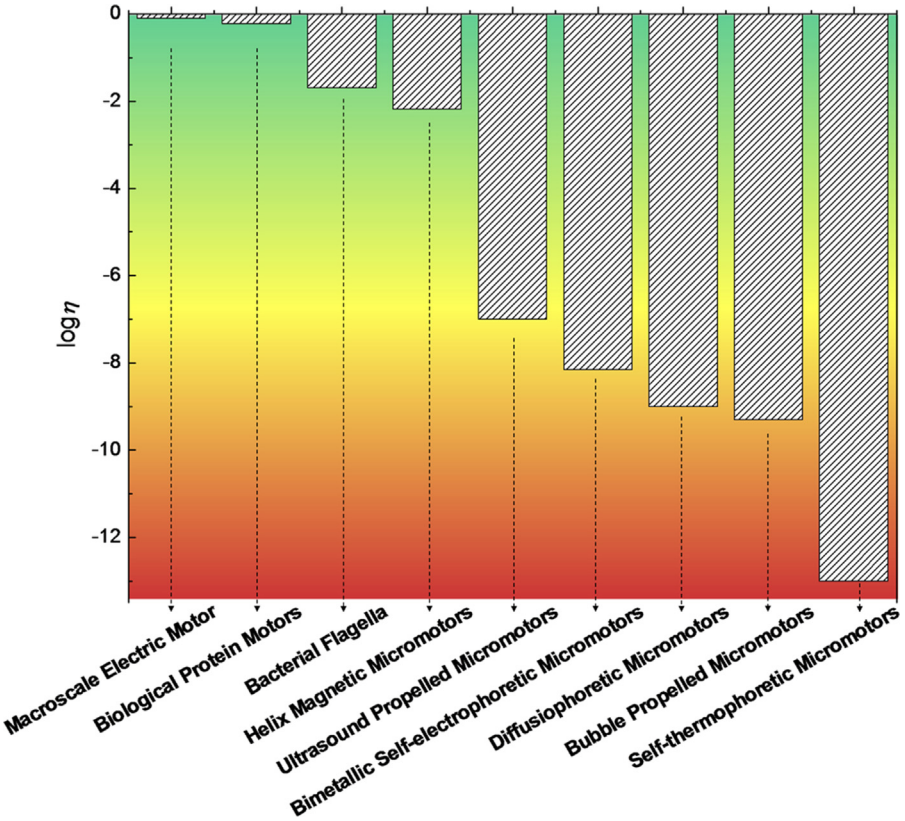

Figure 13 Comparison of the energy efficiency (η) of different types of nano- and micromotors. The values plotted logarithmically are: electric motor 80% (rough estimate), biological protein motor (kinesin) 60% [128,129], bacterial flagella 2% [130], helical magnetic micromotors 0.66% (During the estimation of this energy efficiency the energy absorbed by the medium was not considered. Therefore 0.66% is the upper limit of the true efficiency. The detail of this estimate can be found in Ref. [81]), acoustically propelled metallic micromotors on the order of 10^{-7} [81], Au—Pt catalytic micromotors 7×10^{-9} [30,81], micron sized diffusiophoretic motors on the order of 10^{-9} [127], bubble propelled micromotors 5×10^{-10} [81], and self-thermophoretic micromotors on the order of 10^{-13} [81]. The color shading runs from highest (green) to lowest (red) efficiency.

mechanism is not as well understood in the latter case. Hong et al. postulated that because catalytic motors diffuse faster at higher fuel concentrations, they should preferentially diffuse up concentration gradients of fuel [133]. When Pt/Au nanorods were placed in a gradient of hydrogen peroxide, the rods gradually diffused to the high concentration region where they exhibited higher diffusivity (Fig. 14). A similar phenomenon was also discovered in the polymerization motor system mentioned above [93]; those motors move toward regions of higher monomer concentration.

Nano- and micromotors propelled by self-generated chemical gradients can also exhibit chemotaxis in response to each others' gradients. According to classical DLVO theory [136,137], interactions between colloidal particles arise from a combination of van der Waals forces (generally attractive) and electrostatic interactions between double layers. Microparticles that actively generate or consume chemicals establish chemical gradients around them, which, in the case of ionic solutes, also generate electric fields by diffusiophoresis. In general the spatial extent of these fields is very large — roughly the diffusion length scale of tens to hundreds of microns — relative to DLVO forces, which become important at distances of a few microns. The self-generated electric fields drive the electrophoresis of

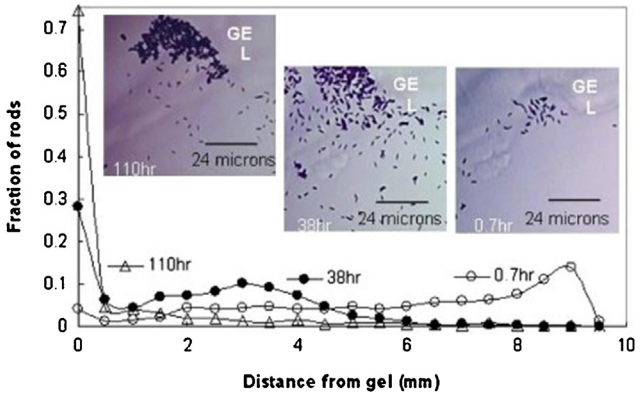

Figure 14 The changing distribution of Pt—Au rods in a H_2O_2 concentration gradient. The gel (soaked in 30% H_2O_2) appears in the upper part. The images were taken at 0.7 h, 38 h, and 110 h. The fraction of rods was evaluated by dividing the number of rods in a frame at a certain distance by the total number, summed over the frames at all distances. Insets show the change in population of Pt—Au rods near the gel, visualized under bright field inverse microscopy.
The images are taken from Ref. [135] with permission from The American Physics Society.

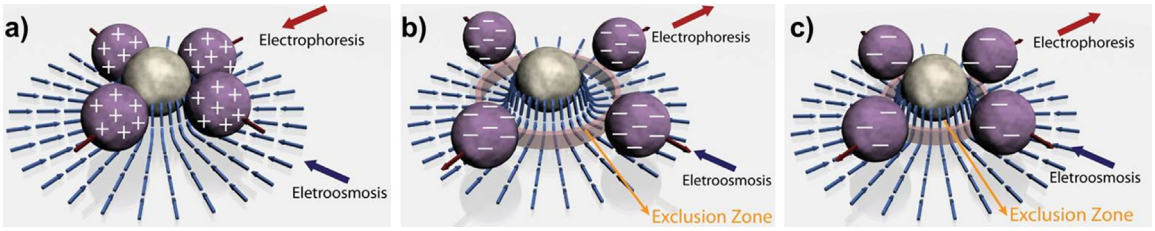

Figure 15 Schemes for diffusiophoretic interaction between the central particle and nearby particles with an inward electric field [86]. (a) When the nearby particles are positively charged, the directions of electrophoresis and electroosmosis are both inwards, the diffusiophoretic interactions are attractive, and the system shows a ''schooling'' pattern. (b) When the nearby particles are negatively charged and $\zeta_P > \zeta_w$, outward electrophoresis dominates over inward electroosmosis. The diffusiophoretic interaction is thus repulsive, and the system shows ''exclusion'' patterns. (c) When the nearby particles are negatively charged and $\zeta_P > \zeta_w$, inward electroosmosis dominates and the diffusiophoretic interaction is attractive. Therefore the system shows ''schooling'' patterns. However, when the particles come close enough to the central one, the repulsive electrophoretic force dominates again due to vanishing electroosmotic flow, and small exclusion zones are formed between the central particle and nearby particles.

nearby particles as well as electroosmotic flow along the surface of the substrate, where the motion of dense particles is typically imaged. The zeta potentials of the particles and substrate determine the relative magnitudes of electrophoresis and electroosmosis, which can occur in the same or opposite directions. Fig. 15 illustrates how cooperative behavior arises from these interactions.

Based on diffusiophoretic interactions, it is possible for the particles to respond collectively to external stimuli, *i.e.* particles can cluster and hence show ''schooling'' behavior [85], or disperse and hence exhibit ''exclusion'' behavior. These collective behaviors usually occur when particles are close enough that the gradients of their secreted chemicals converge. Sen et al. studied the factors that influence the propensity of schooling behavior through numerical modeling, and found that high particle number density, high zeta potential, fast ion secretion rates, and slow Brownian motion all aid in the formation of collective patterns [89]. Duan et al. later experimentally quantified the effect of particle number density on the diffusion of powered silver halide particles [94].

Ibele et al. discovered that silver chloride microparticles, when placed under UV light, form ''schools'' as described above [25]. When negatively charged, passive silica particles were added to this system, they responded to fields generated by the active AgCl particles in a kind of predator–prey interaction. Electroosmotic flow generated at the AgCl particles drives the silica particles toward them and eventually they are surrounded (Fig. 16). However, the repulsive electrophoretic force creates an exclusion zone around the AgCl

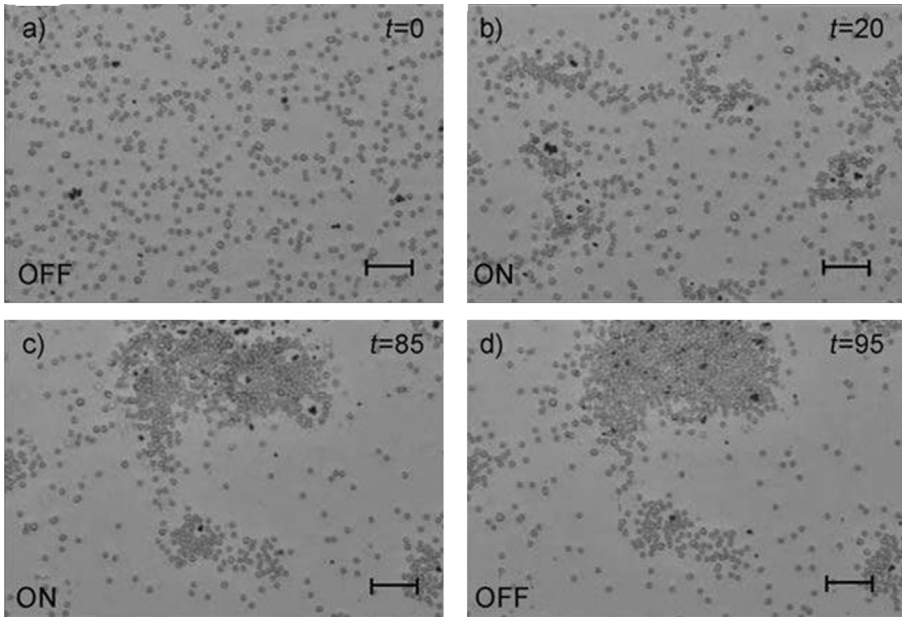

Figure 16 ''Predator–prey'' behavior of active AgCl (prey, darker objects) and passive silica spheres (predator) [25]. (a) Without UV light, particles are randomly dispersed (b, c) When illuminated with UV light the silica spheres actively surround their prey, and an exclusion zone is seen around the AgCl particles. (d) The exclusion zone disappears when UV light is turned off. Times (*t*; seconds) are given in the upper right corner. Scale bars: 20 μm.

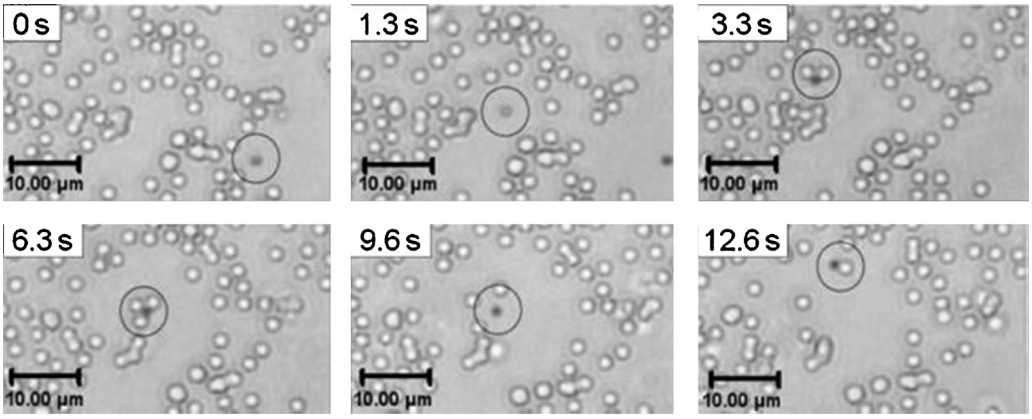

Figure 17 Time-lapse optical microscope images of an AgCl particle with silica spheres in 1% (v/v) H_2O_2 solution under UV light [84]. The AgCl particle alternates between attracting and binding nearby silica particles for several seconds, and then releases them and diffuses rapidly before the next binding event. Traveling waves of these oscillatory movements are observed over length scales of hundreds of microns.
Copyright 2010 The American Chemical Society, reprinted with permission.

particles. Once the UV excitation is turned off, the exclusion zone collapses. This system, which has some resemblance to a biological immune response, emerges from simple attractive and repulsive interactions in self-generated electric fields.

Complex collective micromotor systems that show interactions over very long distances can be designed by incorporating other chemical reactions. For example, spatiotemporal oscillation patterns are observed with AgCl and silica particles under UV light in hydrogen peroxide solution [84]. In this system the AgCl motors exhibit an oscillatory attach-release motion with nearby silica spheres, as shown in Fig. 17.

By coupling different reactions, it is possible to design systems that exhibit transitions between different collective behaviors. Silver orthophosphate microparticles (Ag_3PO_4) in aqueous media show transitions between ''exclusion'' and ''schooling'' [86], which are triggered by shifting the chemical equilibrium (by addition or removal of ammonia) or in response to UV light, as shown in Fig. 18.

Interesting interactions between catalytic microrotors have also been observed [40]. The design of the rotors is shown in Fig. 19. These microrods spin about their central point at frequencies of a few Hz in hydrogen peroxide solutions. Co-rotating rotors avoid contact with each other whereas counter-rotating rotors move closer to each other and experience frequent collisions. The mechanism for these dynamic interactions between rotors is still unclear and may originate from the shear forces between the rotors, as well as chemical gradients in the system.

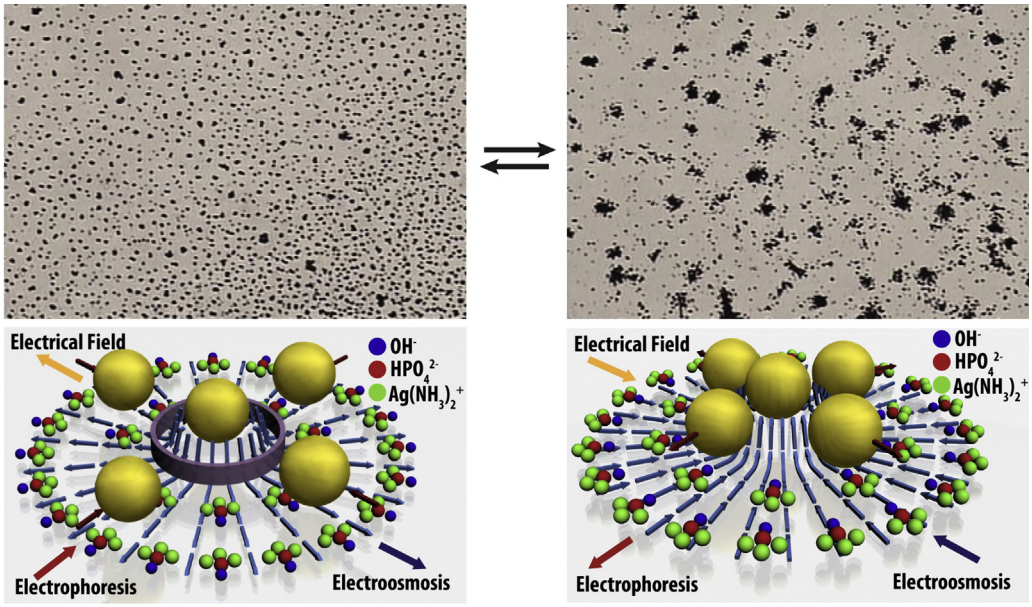

Figure 18 Transition between exclusion and schooling behavior based of silver phosphate particles [86].
Copyright 2013 The American Chemical Society, reprinted with permission.

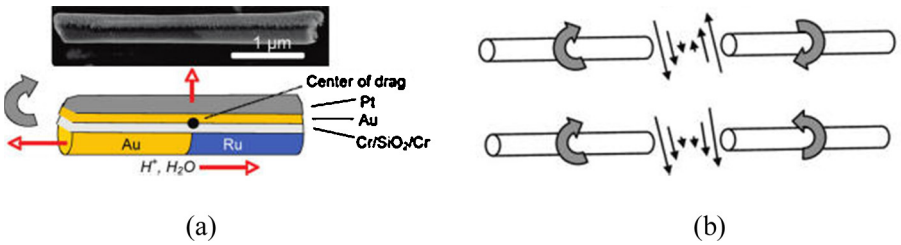

Figure 19 (a) (Top) Field-emission SEM image and cartoon illustration of Au—Ru microrotor; (b) schematic drawing of the fluid velocity distribution between the tips of the microrotors [40].
Copyright 2009 The American Chemical Society, reprinted with permission.

The emergence of complex patterns and collective behavior is interesting in the context of understanding and mimicking the behavior of biological motors such as bacterial colonies and other collections of living cells. The collective behavior of self-electrophoretic motors can in general be rationalized and predicted in terms of simple interaction rules. The study of how these synthetic nano- and micromotors respond to and affect each other may lead to a better understanding of how cells and bacteria communicate with each other. In addition the interactions between particles in self-generated fields, when engineered properly, could lead to useful biomimetic structures that might otherwise be difficult to assemble.

Shape and composition effects on motor behavior

A variety of factors, both external and internal, can affect motor behavior at nano- and microscale. These include environmental parameters noted above (fluid viscosity, permittivity, density), fuel concentration [7,56,134,138,139], and the presence of trace catalytic species [67,79,80].

Because symmetry breaking is a basic requirement for autonomous motion, the physical shape of nano- and micromotors is key factor in their movement [36]. Conventional microfabrication techniques are limited to a few basic

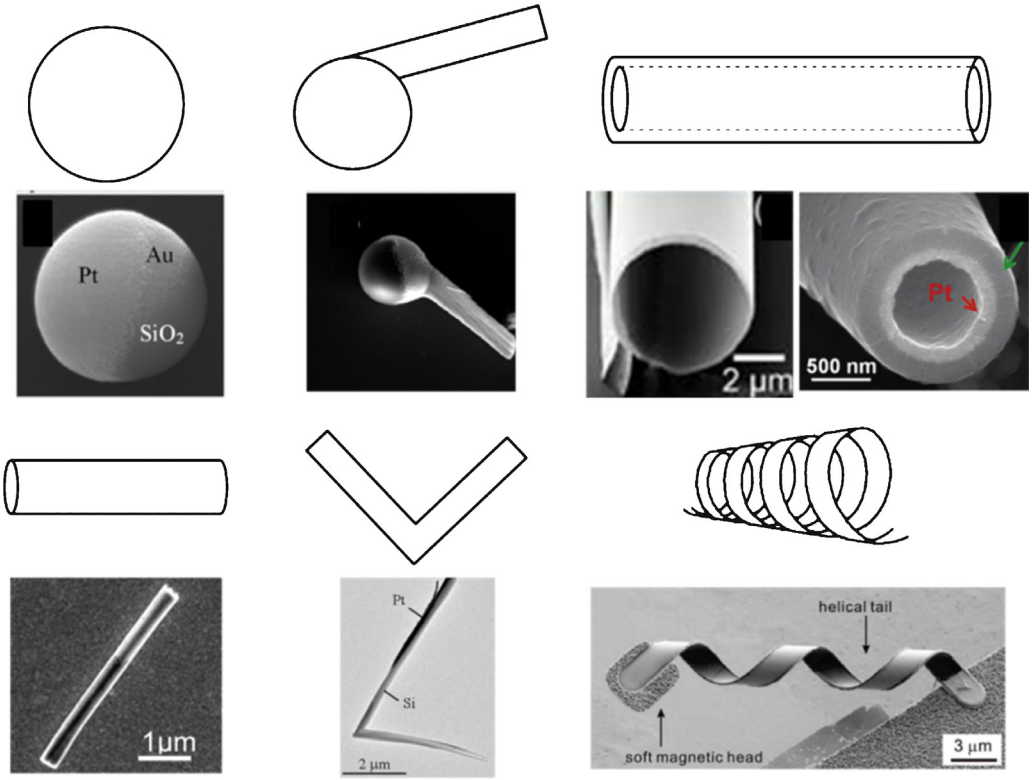

Figure 20 Common shapes used in nano- and micromotor designs. SEM images are presented as actual examples of motors fabricated into these shapes, including spheres [52] (copyright 2010 American Institute of Physics), tadpoles [140] (copyright 2011 The American Chemical Society, reprinted with permission), nano- and micro-rods [49] (copyright 2006 The American Chemical Society, reprinted with permission), microtubes [6,142] (copyright 2009 John Wiley & Sons, Inc., reprinted with permission; 2011 The American Chemical Society, reprinted with permission), V shaped rods [143] (copyright 2007 The American Chemical Society, reprinted with permission) and helices [144] (copyright 2009 The American Chemical Society, reprinted with permission).

shapes including spheres, rods and tubes, and these shapes dominate the literature on nano- and micromotors. By using advanced techniques such as glancing angle deposition, motors of more complicated shapes (such as V shapes and helices) can be fabricated [140,141] (Fig. 20).

The particle size also plays an important role in motor behavior, but our current level of understanding of the scaling issue is quite limited. For example the speed of self-electrophoretic Au—Pt nanomotors in H_2O_2 has been found experimentally to decrease with increasing motor size, both for rod-shaped and for spherical motors [53,145]. This trend has also been observed for Cu—Pt self-electrophoretic nanomotors in Br_2 and I_2 solutions [56]. This is an intriguing observation because intuition as well as the known scaling behavior of larger motors would suggest otherwise [146]. The surface area (therefore propulsion force) scales roughly with the square of particle size, whereas the viscous drag force only scales linearly at low Reynolds number. The speed of self-diffusiophoretic Pt—polystyrene Janus particles in H_2O_2 solution has been found to be either dependent or independent of the particle size in different scaling regimes [95,147]. This has been attributed to the complicated catalytic reaction-diffusion process that is a function of particle size, diffusion coefficient, bulk solute concentration and reaction kinetics.

Nano- and micromotors made of different materials can demonstrate significantly different motion speed, and even reverse their directions. For example, the speed and direction of bimetallic nanomotors driven by self-electrophoresis can be tuned by replacing gold and platinum with a number of other catalytic metals [49]. Their respective mixed potentials for the decomposition of H_2O_2 determine which metal acts at the cathode or anode and to which end the motors move. Nanorods made of different materials show different behaviors in ultrasound, and only rods made of metals exhibit fast directional motion [36]. This is a result of the acoustic contrast between the material and surrounding fluid, which ultimately determines the magnitude of the acoustic radiation force acting on the particle.

Future development of smarter and more effective nano- and micromotors will inevitably call for better control and uniformity in microfabrication. This is a challenging task that requires a more thorough understanding not only of how individual factors affect the motors, but also how they interact. To achieve this level of understanding, it is necessary to revisit the existing nano- and micromotor systems and perform systematic studies on the relevant parameters. In addition, significant progress in both theory and modeling is needed to help advance our knowledge in this area.

Future prospects: from motors to machines

A significant effort in the field of synthetic nano and micromotors is focused on building functioning machines based on motors. After all, colloidal particles that do nothing than move are not particularly useful. To this end, a variety of potentially useful functionalities have been added to different kinds of nano and micromotors. Micromotor systems engineered to behave differently in the presence of certain external stimuli can be used for sensing applications. For example, bimetallic nanomotors that undergo speed changes in the presence of DNA [80], or AgCl particles that school under certain conditions, can be used in analytical applications [25]. Cargo transport and delivery is another popular and potentially useful functionality, especially in the context of particle sorting, drug delivery, cancer detection, and assembly at microscale [65,66,116]. Different mechanisms have been exploited to the transport and delivery of a variety of microparticles including latex microspheres [76], square metallic plates [116], cancer cells [148], and bacteria [149]. More recently it has also been shown that micromotors can act collectively as logic gates when orthogonal chemical and light signals are used as inputs [86]. The principle of particle and fluid movement powered by diffusiophoresis has also been used for enhanced recovery of oil [150].

The prospect of building more complex machines that function at the micro- or even nanoscale has captured the imagination of scientists and science fiction writers for many decades [151—153]. One famous example is the 1959 speech given by Richard Feynman, in which he predicted the flourishing research field of nanoscience and nanotechnology [154]. Feynman's vision, and its later elaboration by Drexler [155]. It was mostly concerned with the concept of machines that could be assembled at the atomic or molecular level. Although there are now many examples of synthetic molecular machines [156], making them atom-by-atom and powering their movement remains very difficult challenges [157]. In the realm of science fiction, which often provides good inspiration for scientific research in the ''real world,'' the 1966 movie *Fantastic Voyage* described a shrinking ray approach to minimally invasive surgery: a human crew was sent into a patient's bloodstream in a miniature submarine to carry out a delicate brain operation, encountering many interesting hazards along the way [158]. The movie identified some likely obstacles, such as attack by the immune system, but neglected others including Brownian motion and the efficiency of propulsion at low Reynolds number.

Research in micro(nano)electromechanical systems (MEMS or NEMS) provides some interesting demonstrations of current efforts to build small machines through a top-down approach [159]. Despite the great success that MEMS and NEMS have enjoyed for building sensors, actuators, accelerometers, mirror arrays, and microfluidic devices, autonomous micro and nanoscale machines have been slow to develop. The difficulty and limitations (in terms of shapes and compositions) of top-down lithographic fabrication rises sharply as the feature size decreases, and the fabrication of three-dimensional objects with moving parts is quite challenging. A few simple kinds of autonomous catalytic motors (*e.g.*, tubular bubble motors) are fabricated lithographically, but in general micromachines made by these techniques have been powered and steered by external fields.

On the other hand, the booming field of nano and micromotor research informs the scientific problem of powered movement on small length scales from a different angle. There is no fundamental reason why these lessons cannot be incorporated into top-down motor design and fabrication. Lithography, including soft lithography and increasingly sophisticated replication techniques, will likely be used in the future to fabricate motors of complicated shapes and

geometries [6,160], enabling more sophisticated control over their behavior and functionality.

If we ask what it will take to implement the medical capability of *Fantastic Voyage*, a shrinking ray seems out of the question. The sizes of atoms and molecules are determined by quantities such as Planck's constant, the masses and charge of fundamental particles, and the permittivity of free space. There is not a lot of wiggle room with these, and nuclear submarines are too expensive for routine surgery anyway. On the other hand, if we consider the functionality required, it is not much more complicated than that of a radio-controlled motorboat. Surgical micro-boats will need to move autonomously, guided by external signals and/or collective interactions with each other. They will need the ability to sense and communicate their environment, as well as to alter it through physical force (*e.g.*, puncturing or cutting cells and tissues), deposition of thermal energy, or delivery of chemical cargo. Many of these functionalities have already been demonstrated, albeit singly and in a limited way, with autonomous motors. The prospect of constructing such motors by massively parallel lithography, with on-board logic and communication capabilities, is a very interesting one that may not be so far in the future.

Beyond biomedicine there are undoubtedly a number of unanticipated applications and technologies that will derive from the concepts learned by studying the mechanisms of powered motion on small length scales. The coupling between sensing and transport should enable new applications such as bottom-up assembly of dynamic structures, roving sensors, ''on-demand'' analyte-triggered cargo delivery at specific locations, and related functions. Furthermore, such material assemblies can accomplish tasks collectively (like a colony of ants) that a single constituent element (a single ant) cannot perform [161,162]. The collective behavior that has already been observed in simple particle systems such as AgCl is mimetic of the swarming of bacteria, mold spores, and insects. In the latter case, hive intelligence can emerge from the interactions of specialized members of the colony. Some minimal requirements for such *intelligent systems* are that they contain (a) information and (b) information processors that can both act on and modify the information. The idea of emergent intelligence, in the context of microfabricated robots, has already been the subject of some engaging (and scary) science fiction [163,164]. Despite the malevolence of the microrobot swarms in *Prey*, or of the humanly misdirected microspiders in *Spiral*, the design of self-assembling systems from which intelligence (and other functions so far associated uniquely with biology) can emerge is among the grand challenges of science. Autonomous micromotors perhaps represent some first steps in this direction.

Acknowledgments

We thank our many coworkers and collaborators who have contributed to this project over the past decade. This research has been conducted in the *Penn State Center for Nanoscale Science*, a Materials Research Science and Engineering Center supported by the National Science Foundation under grant DMR-0820404.

References

[1] Kebes, Kinesin Cartoon. <http://en.wikipedia.org/wiki/File:Kinesin_cartoon.png/>, 2013 (accessed 03.07.13).
[2] Bact, EscherichiaColi NIAID. <http://en.wikipedia.org/wiki/File:EscherichiaColi_NIAID.jpg/>, 2013 (accessed 03.07.13).
[3] F.J. Harrison, *Coccinella transversalis* 2. <http://en.wikipedia.org/wiki/File:Coccinella_transversalis_2.jpg/>, 2013 (accessed 03.07.13).
[4] D. Vinci, Quibik, Uomo Vitruviano. <http://en.wikipedia.org/wiki/File:Uomo_Vitruviano.jpg/>, 2013 (accessed 03.07.13).
[5] Y. Shirai, A.J. Osgood, Y. Zhao, K.F. Kelly, J.M. Tour, Nano Lett. 5 (2005) 2330—2334.
[6] A.A. Solovev, Y. Mei, E. Bermúdez Ureña, G. Huang, O.G. Schmidt, Small 5 (2009) 1688—1692.
[7] W.F. Paxton, K.C. Kistler, C.C. Olmeda, A. Sen, S.K. St Angelo, Y. Cao, T.E. Mallouk, P.E. Lammert, V.H. Crespi, J. Am. Chem. Soc. 126 (2004) 13424—13431.
[8] K.Y. Ma, P. Chirarattananon, S.B. Fuller, R.J. Wood, Science 340 (2013) 603—607.
[10] E.M. Purcell, Am. J. Phys. 45 (1977) 3—11.
[11] H. Masoud, B.I. Bingham, A. Alexeev, Soft Matter 8 (2012) 8944—8951.
[12] T. Sanchez, D. Welch, D. Nicastro, Z. Dogic, Science 333 (2011) 456—459.
[13] V. Chan, K. Park, M.B. Collens, H. Kong, T.A. Saif, R. Bashir, Sci. Rep. UK 2 (2012).
[14] W.R. Browne, B.L. Feringa, Nat. Nanotechnol. 1 (2006) 25—35.
[15] A. Goel, V. Vogel, Nat. Nanotechnol. 3 (2008) 465—475.
[16] P. Calvo-Marzal, S. Sattayasamitsathit, S. Balasubramanian, J.R. Windmiller, C. Dao, J. Wang, Chem. Commun. (Camb.) 46 (2010) 1623—1624.
[17] S.T. Chang, E. Beaumont, D.N. Petsev, O.D. Velev, Lab Chip 8 (2008) 117—124.
[18] G. Loget, A. Kuhn, Nat. Commun. 2 (2011) 535.
[19] R. Dreyfus, J. Baudry, M.L. Roper, M. Fermigier, H.A. Stone, J. Bibette, Nature 437 (2005) 862—865.
[20] W. Gao, S. Sattayasamitsathit, K.M. Manesh, D. Weihs, J. Wang, J. Am. Chem. Soc. 132 (2010) 14403—14405.
[21] A. Ghosh, P. Fischer, Nano Lett. 9 (2009) 2243—2245.
[22] S. Tottori, L. Zhang, F. Qiu, K.K. Krawczyk, A. Franco-Obregon, B.J. Nelson, Adv. Mater. 24 (2012) 811—816.
[23] F.M. Hoelscher, Fish school. <http://en.wikipedia.org/wiki/File:Fish_school.jpg/>, 2013 (accessed 03.07.13).
[24] A. Rae, Quelea Flock. <http://en.wikipedia.org/wiki/File:Red-billed_quelea_flocking_at_waterhole.jpg/>, 2013 (accessed 02.07.13).
[25] M. Ibele, T.E. Mallouk, A. Sen, Angew. Chem. Int. Ed. 48 (2009) 3308—3312.
[26] Y. Wang, S.T. Fei, Y.M. Byun, P.E. Lammert, V.H. Crespi, A. Sen, T.E. Mallouk, J. Am. Chem. Soc. 131 (2009) 9926—9927.
[27] T.R. Kline, W.F. Paxton, Y. Wang, D. Velegol, T.E. Mallouk, A. Sen, J. Am. Chem. Soc. 127 (2005) 17150—17151.
[28] J.J. McDermott, A. Kar, M. Daher, S. Klara, G. Wang, A. Sen, D. Velegol, Langmuir 28 (2012) 15491—15497.
[29] I.K. Jun, H. Hess, Adv. Mater. 22 (2010) 4823—4825.
[30] W.F. Paxton, P.T. Baker, T.R. Kline, Y. Wang, T.E. Mallouk, A. Sen, J. Am. Chem. Soc. 128 (2006) 14881—14888.
[31] M.E. Ibele, Y. Wang, T.R. Kline, T.E. Mallouk, A. Sen, J. Am. Chem. Soc. 129 (2007) 7762—7763.
[32] Y. Hong, M. Diaz, U.M. Córdova-Figueroa, A. Sen, Adv. Funct. Mater. 20 (2010) 1568—1576.
[33] H. Zhang, K. Yeung, J.S. Robbins, R.A. Pavlick, M. Wu, R. Liu, A. Sen, S.T. Phillips, Angew. Chem. Int. Ed. 51 (2012) 2400—2404.

[34] V. Yadav, H. Zhang, R. Pavlick, A. Sen, J. Am. Chem. Soc. 134 (2012) 15688—15691.
[35] J.G. Gibbs, Y.P. Zhao, Appl. Phys. Lett. 94 (2009) 163103—163104.
[36] W. Wang, L.A. Castro, M. Hoyos, T.E. Mallouk, ACS Nano 6 (2012) 6122—6132.
[37] T. Mirkovic, N.S. Zacharia, G.D. Scholes, G.A. Ozin, Small 6 (2010) 159—167.
[38] L.D. Qin, M.J. Banholzer, X.Y. Xu, L. Huang, C.A. Mirkin, J. Am. Chem. Soc. 129 (2007) 14870—14871.
[39] S. Fournier-Bidoz, A.C. Arsenault, I. Manners, G.A. Ozin, Chem. Commun. (2005) 441—443.
[40] Y. Wang, S.-t. Fei, Y.-M. Byun, P.E. Lammert, V.H. Crespi, A. Sen, T.E. Mallouk, J. Am. Chem. Soc. 131 (2009) 9926—9927.
[41] P.H. Jones, F. Palmisano, F. Bonaccorso, P.G. Gucciardi, G. Calogero, A.C. Ferrari, O.M. Marago, ACS Nano 3 (2009) 3077—3084.
[42] B. Edwards, T.S. Mayer, R.B. Bhiladvala, Nano Lett. 6 (2006) 626—632.
[43] K. Keshoju, H. Xing, L. Sun, Appl. Phys. Lett. 91 (2007).
[44] Y. Solomentsev, J.L. Anderson, J. Fluid Mech. 279 (1994) 197—215.
[45] J.L. Anderson, Annu. Rev. Fluid Mech. 21 (1989) 61—99.
[46] N.I. Kovtyukhova, J. Phys. Chem. C 112 (2008) 6049—6056.
[47] W.F. Paxton, A. Sen, T.E. Mallouk, Chem. Eur. J. 11 (2005) 6462—6470.
[48] T.R. Kline, J. Iwata, P.E. Lammert, T.E. Mallouk, A. Sen, D. Velegol, J. Phys. Chem. B 110 (2006) 24513—24521.
[49] Y. Wang, R.M. Hernandez, D.J. Bartlett, J.M. Bingham, T.R. Kline, A. Sen, T.E. Mallouk, Langmuir 22 (2006) 10451—10456.
[50] J.L. Moran, J.D. Posner, J. Fluid Mech. 680 (2011) 31—66.
[51] E. Yariv, Proc. R. Soc. A: Math. Phys. Eng. Sci. 467 (2010) 1645—1664.
[52] J.G. Gibbs, N.A. Fragnito, Y. Zhao, Appl. Phys. Lett. 97 (2010) 253107.
[53] P.M. Wheat, N.A. Marine, J.L. Moran, J.D. Posner, Langmuir 26 (2010) 13052—13055.
[54] J.M. Catchmark, S. Subramanian, A. Sen, Small 1 (2005) 202—206.
[55] P.J. Li, Z.M. Liao, X.Z. Zhang, X.J. Zhang, H.C. Zhu, J.Y. Gao, K. Laurent, Y. Leprince-Wang, N. Wang, D.P. Yu, Nano Lett. 9 (2009) 2513—2518.
[56] R. Liu, A. Sen, J. Am. Chem. Soc. 133 (2011) 20064—20067.
[57] Y. Yoshizumi, Y. Date, K. Ohkubo, M. Yokokawa, H. Suzuki, 2013 IEEE 26th International Conference on Micro Electro Mechanical Systems (MEMS), 2013, pp. 540—543.
[58] N. Mano, A. Heller, J. Am. Chem. Soc. 127 (2005) 11574—11575.
[59] N.S. Zacharia, Z.S. Sadeq, G.A. Ozin, Chem. Commun. (Camb.) (2009) 5856—5858.
[60] S. Sanchez, M. Pumera, Chem. Asian J. 4 (2009) 1402—1410.
[61] W. Gao, S. Sattayasamitsathit, J. Wang, Chem. Rec. 12 (2012) 224—231.
[62] S. Sattayasamitsathit, W. Gao, P. Calvo-Marzal, K.M. Manesh, J. Wang, Chemphyschem 11 (2010) 2802—2805.
[63] U.K. Demirok, R. Laocharoensuk, K.M. Manesh, J. Wang, Angew. Chem. Int. Ed. 47 (2008) 9349—9351.
[64] R. Laocharoensuk, J. Burdick, J. Wang, ACS Nano 2 (2008) 1069—1075.
[65] J. Wang, Lab Chip 12 (2012) 1944—1950.
[66] D. Patra, S. Sengupta, W.T. Duan, H. Zhang, R. Pavlick, A. Sen, Nanoscale 5 (2013) 1273—1283.
[67] S. Campuzano, D. Kagan, J. Orozco, J. Wang, Analyst 136 (2011) 4621—4630.
[68] P. Calvo-Marzal, K.M. Manesh, D. Kagan, S. Balasubramanian, M. Cardona, G.U. Flechsig, J. Posner, J. Wang, Chem. Commun. (2009) 4509—4511.
[69] S. Balasubramanian, D. Kagan, K.M. Manesh, P. Calvo-Marzal, G.U. Flechsig, J. Wang, Small 5 (2009) 1569—1574.
[70] T.R. Kline, W.F. Paxton, T.E. Mallouk, A. Sen, Angew. Chem. Int. Ed. Engl. 44 (2005) 744—746.
[71] N. Chaturvedi, Y. Hong, A. Sen, D. Velegol, Langmuir 26 (2010) 6308—6313.
[72] P. Dhar, Y.Y. Cao, T. Kline, P. Pal, C. Swayne, T.M. Fischer, B. Miller, T.E. Mallouk, A. Sen, T.H. Johansen, J. Phys. Chem. C 111 (2007) 3607—3613.
[73] W. Gao, K.M. Manesh, J. Hua, S. Sattayasamitsathit, J. Wang, Small 7 (2011) 2047—2051.
[74] J. Burdick, R. Laocharoensuk, P.M. Wheat, J.D. Posner, J. Wang, J. Am. Chem. Soc. 130 (2008) 8164—8165.
[75] W. Gao, D. Kagan, O.S. Pak, C. Clawson, S. Campuzano, E. Chuluun-Erdene, E. Shipton, E.E. Fullerton, L.F. Zhang, E. Lauga, J. Wang, Small 8 (2012) 460—467.
[76] S. Sundararajan, P.E. Lammert, A.W. Zudans, V.H. Crespi, A. Sen, Nano Lett. 8 (2008) 1271—1276.
[77] S. Sundararajan, S. Sengupta, M.E. Ibele, A. Sen, Small 6 (2010) 1479—1482.
[78] D. Kagan, R. Laocharoensuk, M. Zimmerman, C. Clawson, S. Balasubramanian, D. Kang, D. Bishop, S. Sattayasamitsathit, L. Zhang, J. Wang, Small 6 (2010) 2741—2747.
[79] D. Kagan, P. Calvo-Marzal, S. Balasubramanian, S. Sattayasamitsathit, K.M. Manesh, G.U. Flechsig, J. Wang, J. Am. Chem. Soc. 131 (2009) 12082—12083.
[80] J. Wu, S. Balasubramanian, D. Kagan, K.M. Manesh, S. Campuzano, J. Wang, Nat. Commun. 1 (2010) 36.
[81] W. Wang, T.-Y. Chiang, D. Velegol, T.E. Mallouk, J. Am. Chem. Soc. 135 (2013) 1280—1283.
[82] J.L. Anderson, Annu. Rev. Fluid Mech. 21 (1989) 61.
[83] J.P. Ebel, J.L. Anderson, D.C. Prieve, Langmuir 4 (1988) 396—406.
[84] M.E. Ibele, P.E. Lammert, V.H. Crespi, A. Sen, ACS Nano 4 (2010) 4845—4851.
[85] D. Kagan, S. Balasubramanian, J. Wang, Angew. Chem. Int. Ed. 50 (2011) 503—506.
[86] W. Duan, R. Liu, A. Sen, J. Am. Chem. Soc. 135 (2013) 1280—1283.
[87] J. Palacci, S. Sacanna, A.P. Steinberg, D.J. Pine, P.M. Chaikin, Science 339 (2013) 936—940.
[88] A. Reinmüller, E.C. Oğuz, R. Messina, H. Löwen, H.J. Schöpe, T. Palberg, J. Chem. Phys. 136 (2012) 164505.
[89] A. Sen, M. Ibele, Y. Hong, D. Velegol, Faraday Discuss. 143 (2009) 15—27.
[90] U.M. Córdova-Figueroa, J.F. Brady, Phys. Rev. Lett. 100 (2008) 158303.
[91] R. Golestanian, Phys. Rev. Lett. 102 (2009) 188305.
[92] P.O. Staffeld, J.A. Quinn, J. Colloid Interface Sci. 130 (1989) 88—100.
[93] R.A. Pavlick, S. Sengupta, T. McFadden, H. Zhang, A. Sen, Angew. Chem. Int. Ed. 50 (2011) 9374—9377.
[94] W. Duan, M. Ibele, R. Liu, A. Sen, Eur. Phys. J. E 35 (2012) 1—8.
[95] J.R. Howse, R.A.L. Jones, A.J. Ryan, T. Gough, R. Vafabakhsh, R. Golestanian, Phys. Rev. Lett. 99 (2007) 048102.
[96] H. Ke, S. Ye, R.L. Carroll, K. Showalter, J. Phys. Chem. A 114 (2010) 5462—5467.
[97] J. Wang, W. Gao, ACS Nano 6 (2012) 5745—5751.
[98] B.J. Nelson, I.K. Kaliakatsos, J.J. Abbott, Annu. Rev. Biomed. Eng. 12 (2010) 55—85.
[99] S.T. Chang, V.N. Paunov, D.N. Petsev, O.D. Velev, Nat. Mater. 6 (2007) 235—240.
[100] S.B. Barnett, G.R. Ter Haar, M.C. Ziskin, H.-D. Rott, F.A. Duck, K. Maeda, Ultrasound Med. Biol. 26 (2000) 355—366.

[101] D.L. Miller, N.B. Smith, M.R. Bailey, G.J. Czarnota, K. Hynynen, I.R.S. Makin, A.I.U. Med, B. Comm, J. Ultrasound Med. 31 (2012) 623—634.
[102] A. Kundt, O. Lehman, Ann. Phys. (1874) 1.
[103] J. Friend, L.Y. Yeo, Rev. Mod. Phys. 83 (2011) 647—704.
[104] X.Y. Ding, S.C.S. Lin, B. Kiraly, H.J. Yue, S.X. Li, I.K. Chiang, J.J. Shi, S.J. Benkovic, T.J. Huang, Proc. Natl. Acad. Sci. U.S.A. 109 (2012) 11105—11109.
[105] A. Lenshof, C. Magnusson, T. Laurell, Lab Chip 12 (2012) 1210—1223.
[106] D. Kagan, M.J. Benchimol, J.C. Claussen, E. Chuluun-Erdene, S. Esener, J. Wang, Angew. Chem. Int. Ed. 51 (2012) 7519—7522.
[107] A. Albanese, P.S. Tang, W.C.W. Chan, Annu. Rev. Biomed. Eng. 14 (2012) 1—16.
[108] S. Mitragotri, J. Lahann, Adv. Mater. (Weinheim, Germany) 24 (2012) 3717—3723.
[109] S.N. Rasuli, R. Golestanian, J. Phys. Condens Mater. 17 (2005) S1171—S1176.
[110] H.R. Jiang, N. Yoshinaga, M. Sano, Phys. Rev. Lett. 105 (2010) 268302.
[111] L. Baraban, R. Streubel, D. Makarov, L. Han, D. Karnaushenko, O.G. Schmidt, G. Cuniberti, ACS Nano 7 (2012) 1360—1367.
[112] B. Qian, D. Montiel, A. Bregulla, F. Cichos, H. Yang, Chem. Sci. 4 (2013) 1420—1429.
[113] R. Golestanian, Phys. Rev. Lett. 108 (2012).
[114] M.C. Yang, M. Ripoll, Phys. Rev. E 84 (2011).
[115] D.A. Wilson, R.J.M. Nolte, J.C.M. van Hest, Nat. Chem. 4 (2012) 268—274.
[116] A.A. Solovev, S. Sanchez, M. Pumera, Y.F. Mei, O.G. Schmidt, Adv. Funct. Mater. 20 (2010) 2430—2435.
[117] A.A. Solovev, W. Xi, D.H. Gracias, S.M. Harazim, C. Deneke, S. Sanchez, O.G. Schmidt, ACS Nano 6 (2012) 1751—1756.
[118] Y. Mei, A.A. Solovev, S. Sanchez, O.G. Schmidt, Chem. Soc. Rev. 40 (2011) 2109—2119.
[119] G.S. Huang, J.S. Wang, Y.F. Mei, J. Mater. Chem. 22 (2012) 6519—6525.
[120] M. Sentic, G. Loget, D. Manojlovic, A. Kuhn, N. Sojic, Angew. Chem. Int. Ed. 51 (2012) 11284—11288.
[121] S. Sengupta, M.E. Ibele, A. Sen, Angew. Chem. Int. Ed. 51 (2012) 8434—8445.
[122] O.S. Pak, W. Gao, J. Wang, E. Lauga, Soft Matter 7 (2011) 8169—8181.
[123] P. Fischer, A. Ghosh, Nanoscale 3 (2011) 557—563.
[124] Y. Shi, L. Huang, D.W. Brenner, J. Chem. Phys. 131 (2009) 014705.
[125] B. Sabass, U. Seifert, J. Chem. Phys. 136 (2012).
[126] Y.G. Tao, R. Kapral, J. Chem. Phys. 131 (2009) 024113.
[127] B. Sabass, U. Seifert, Phys. Rev. Lett. 105 (2010).
[128] S.M. Block, Cell 93 (1998) 5—8.
[129] S. Iwatani, A.H. Iwane, H. Higuchi, Y. Ishii, T. Yanagida, Biochemistry-US 38 (1999) 10318—10323.
[130] T.R. Kline, M. Tian, J. Wang, A. Sen, M.W.H. Chan, T.E. Mallouk, Inorg. Chem. 45 (2006) 7555—7565.
[131] H.S. Muddana, S. Sengupta, T.E. Mallouk, A. Sen, P.J. Butler, J. Am. Chem. Soc. 132 (2010) 2110—2111.
[132] H.C. Berg, D.A. Brown, Nature 239 (1972) 500—504.
[133] Y. Hong, N.M.K. Blackman, N.D. Kopp, A. Sen, D. Velegol, Phys. Rev. Lett. 99 (2007) 178103.
[134] S. Sengupta, K.K. Dey, H.S. Muddana, T. Tabouillot, M.E. Ibele, P.J. Butler, A. Sen, J. Am. Chem. Soc. 135 (2013) 1406—1414.
[135] Y. Hong, N. Blackman, N. Kopp, A. Sen, D. Velegol, Phys. Rev. Lett. 99 (2007).
[136] B.V. Derjaguin, L. Landau, Acta Physicochim. (URSS) (1941) 30.
[137] E.J. Verwey, J.T.G. Overbeek, Theory of the Stability of Lyophobic Colloids, Elsevier, Amsterdam, 1948.
[138] S. Sanchez, A.N. Ananth, V.M. Fomin, M. Viehrig, O.G. Schmidt, J. Am. Chem. Soc. 133 (2011) 14860—14863.
[139] D.A. Wilson, B. de Nijs, A. van Blaaderen, R.J.M. Nolte, J.C.M. van Hest, Nanoscale 5 (2013) 1315—1318.
[140] J.G. Gibbs, S. Kothari, D. Saintillan, Y.P. Zhao, Nano Lett. 11 (2011) 2543—2550.
[141] J.G. Gibbs, Y.P. Zhao, Small 5 (2009) 2304—2308.
[142] W. Gao, S. Sattayasamitsathit, J. Orozco, J. Wang, J. Am. Chem. Soc. 133 (2011) 11862—11864.
[143] Y.P. He, J.S. Wu, Y.P. Zhao, Nano Lett. 7 (2007) 1369—1375.
[144] L. Zhang, J.J. Abbott, L. Dong, K.E. Peyer, B.E. Kratochvil, H. Zhang, C. Bergeles, B.J. Nelson, Nano Lett. 9 (2009) 3663—3667.
[145] P. Dhar, T.M. Fischer, Y. Wang, T.E. Mallouk, W.F. Paxton, A. Sen, Nano Lett. 6 (2006) 66—72.
[146] J.H. Marden, L.R. Allen, Proc. Natl. Acad. Sci. U.S.A. 99 (2002) 4161—4166.
[147] S. Ebbens, M.H. Tu, J.R. Howse, R. Golestanian, Phys. Rev. E 85 (2012).
[148] S. Balasubramanian, D. Kagan, C.-M. Jack Hu, S. Campuzano, M.J. Lobo-Castañon, N. Lim, D.Y. Kang, M. Zimmerman, L. Zhang, J. Wang, Angew. Chem. Int. Ed. 50 (2011) 4161—4164.
[149] S. Campuzano, J. Orozco, D. Kagan, M. Guix, W. Gao, S. Sattayasamitsathit, J.C. Claussen, A. Merkoçi, J. Wang, Nano Lett. 12 (2011) 396—401.
[150] A. Sen, Abstr. Pap. Am. Chem. Soc. 241 (2011).
[151] G.M. Whitesides, Sci. Am. 285 (2001) 78—83.
[152] J. Wang, ACS Nano 3 (2009) 4—9.
[153] G.A. Ozin, I. Manners, S. Fournier-Bidoz, A. Arsenault, Adv. Mater. (Weinheim, Germany) 17 (2005) 3011—3018.
[154] R.P. Feynman, Eng. Sci. 23 (1960) 22—36.
[155] K.E. Drexler, Engines of Creation: The Coming Era of Nanotechnology, Doubleday, New York, 1986.
[156] H. Hess, Soft Matter 2 (2006) 669—677.
[157] R.E. Smalley, Sci. Am. 285 (2001) 76—77.
[158] S. Fleischer, Twentieth Century Fox Film Corporation, 1966.
[159] Microelectronics to Nanoelectronics: Materials, in: Devices & Manufacturability, CRC Press, Boca Raton, 2012.
[160] S. Tottori, L. Zhang, F. Qiu, K.K. Krawczyk, A. Franco-Obregón, B.J. Nelson, Adv. Mater. (Weinheim, Germany) 24 (2012) 709.
[161] A. Deutsch, G. Theraulaz, T. Vicsek, Interface Focus 2 (2012) 689—692.
[162] E. Bonabeau, G. Theraulaz, M. Dorigo, Swarm Intelligence: From Natural to Artificial Systems, Oxford University Press, New York, 1999.
[163] M. Crichton, Prey, HarperCollins Publishers, 2009.
[164] P. McEuen, Spiral, Random House, New York, 2011.

Wei Wang received his B.Sc. in applied chemistry from Harbin Institute of Technology (China) in 2008. He is currently a Ph.D. candidate in the Mallouk Group in the Department of Chemistry at Penn State University. His research focuses on nano- and microscale motors propelled by self-generated forces such as self-electrophoretic and acoustophoretic motors. He is also interested in understanding and predicting the behaviors of these motors through numerical simulations.

Wentao Duan received his B.S. degree in Chemistry at Yuanpei College, Peking University (P.R. China). He then joined the nanomotor research group at the Pennsylvania State University to pursue his Ph.D. degree under the supervision of Prof. Ayusman Sen. His research interests include designing nanomotors that exhibit collective behavior, and exploring and modeling the diffusional properties of nanomotors.

Suzanne Ahmed received her B.S. from the University of California, Riverside and her M.S. in Chemistry from the University of California, Berkeley. She is currently a Ph.D. candidate in the Mallouk Group at Penn State University. Her research focuses on the study of propulsion and control of nano- and microscale motors.

Thomas Mallouk received his Sc.B. from Brown University and his Ph.D. in Chemistry from the University of California, Berkeley. He was a postdoctoral fellow at MIT and a member of the Chemistry faculty at the University of Texas at Austin. Since 1993 he has been at Penn State, where he is now Evan Pugh Professor of Materials Chemistry and Physics. He is interested in the synthesis of solid state compounds and nanomaterials, and their applications in electrochemical and solar energy conversion, microelectronics, catalysis, environmental remediation, and powered motion on the nano- and microscale.

Ayusman Sen was born in Calcutta, India and holds a Ph.D. from the University of Chicago where he was first introduced to catalysis. Following a year of postdoctoral work at the California Institute of Technology, he joined the Chemistry Department of the Pennsylvania State University where he is currently a Distinguished Professor. He is a Fellow of the American Association for the Advancement of Science. His research interests encompass catalysis, organometallic and polymer chemistry, and nanotechnology. He is the author of approximately 325 scientific publications and holds 24 patents. Sen's pastime centers on enological and gastronomical explorations.